Interpretation of TOMS observations of tropical tropospheric ozone with a global model and in situ observations

Randall V. Martin, Daniel J. Jacob, Jennifer A. Logan, Isabelle Bey,[1]
Robert M. Yantosca, Amanda C. Staudt,[2] Qinbin Li, Arlene M. Fiore,
Bryan N. Duncan,[1] and Hongyu Liu
Division of Engineering and Applied Sciences and Department of Earth and Planetary Sciences, Harvard University, Cambridge, Massachusetts, USA

Paul Ginoux[3]
School of Earth and Atmospheric Sciences, Georgia Institute of Technology, Atlanta, Georgia, USA

Valerie Thouret
Laboratoire d'Aérologie CNRS (UMR 5500), Toulouse, France

[1] We interpret the distribution of tropical tropospheric ozone columns (TTOCs) from the Total Ozone Mapping Spectrometer (TOMS) by using a global three-dimensional model of tropospheric chemistry (GEOS-CHEM) and additional information from in situ observations. The GEOS-CHEM TTOCs capture 44% of the variance of monthly mean TOMS TTOCs from the convective cloud differential method (CCD) with no global bias. Major discrepancies are found over northern Africa and south Asia where the TOMS TTOCs do not capture the seasonal enhancements from biomass burning found in the model and in aircraft observations. A characteristic feature of these northern tropical enhancements, in contrast to southern tropical enhancements, is that they are driven by the lower troposphere where the sensitivity of TOMS is poor due to Rayleigh scattering. We develop an efficiency correction to the TOMS retrieval algorithm that accounts for the variability of ozone in the lower troposphere. This efficiency correction increases TTOCs over biomass burning regions by 3–5 Dobson units (DU) and decreases them by 2–5 DU over oceanic regions, improving the agreement between CCD TTOCs and in situ observations. Applying the correction to CCD TTOCs reduces by $\sim$5 DU the magnitude of the "tropical Atlantic paradox" [*Thompson et al.*, 2000], i.e. the presence of a TTOC enhancement over the southern tropical Atlantic during the northern African biomass burning season in December–February. We reproduce the remainder of the paradox in the model and explain it by the combination of upper tropospheric ozone production from lightning NO_x, persistent subsidence over the southern tropical Atlantic as part of the Walker circulation, and cross-equatorial transport of upper tropospheric ozone from northern midlatitudes in the African "westerly duct." These processes in the model can also account for the observed 13–17 DU persistent wave-1 pattern in TTOCs with a maximum over the tropical Atlantic and a minimum over the tropical Pacific during all seasons. The photochemical effects of mineral dust have only a minor role on the modeled distribution of TTOCs, including over northern Africa, due to multiple competing effects. The photochemical effects of mineral dust globally decrease annual mean OH concentrations by 9%. A global lightning NO_x source of 6 Tg N yr^{-1} in the model produces a simulation that is most consistent with TOMS and in situ observations. *INDEX TERMS:* 0343 Atmospheric Composition and Structure: Planetary atmospheres (5405, 5407, 5409, 5704, 5705, 5707); 0365 Atmospheric Composition and Structure: Troposphere—composition and chemistry;

---

[1]Now at Ecole Polytechnique Federale de Lausanne, Switzerland.
[2]Now at National Academy of Sciences, Washington, D. C., USA.
[3]Now at NASA Goddard Space Flight Center, Greenbelt, Maryland, USA.

1. Introduction

[2] Tropical tropospheric ozone plays a key role in determining the oxidizing power of the atmosphere and is an important greenhouse gas. Production of ozone in the tropical troposphere is believed to be controlled by the supply of nitrogen oxide radicals ($NO_x \equiv NO_2 + NO$) originating from lightning, biomass burning, and soils [*Jacob et al.*, 1996]. Considerable uncertainty exists in the factors controlling the distribution of tropical tropospheric ozone, including the roles of biomass burning, lightning, and dynamics [*Thompson et al.*, 2000, 2001]. Starting from the early work of *Fishman et al.* [1990], a number of investigators have used satellite observations from the Total Ozone Mapping Spectrometer (TOMS) to retrieve global distributions of tropical tropospheric ozone columns (TTOCs). In this paper we place the TOMS TTOCs in the context of in situ observations and a global three-dimensional (3-D) model of tropospheric chemistry to understand the factors controlling the distribution of tropical tropospheric ozone.

[3] The TOMS instrument measures solar ultraviolet radiation backscattered from the Earth's surface, the atmosphere, aerosols, and clouds. The standard TOMS retrieval algorithm determines total ozone columns by comparing measured backscattered radiances with calculated radiances for an assumed ozone profile [*McPeters et al.*, 1998]. Strong scattering in the troposphere impairs the sensitivity of TOMS to lower tropospheric ozone and increases the dependence of the reported ozone columns to the assumed tropospheric ozone profile [*Klenk et al.*, 1982; *Hudson et al.*, 1995; *Wellemeyer et al.*, 1997; *McPeters et al.*, 1998; *Kim et al.*, 2001].

[4] Despite the relative insensitivity of TOMS to lower tropospheric ozone, many have attempted to extract tropospheric ozone columns from TOMS measurements [*Fishman et al.*, 1990; *Hudson and Thompson*, 1998; *Ziemke et al.*, 1998; *Fishman and Balok*, 1999; *Thompson and Hudson*, 1999; *Kim et al.*, 2001; *Newchurch et al.*, 2001a, also Tropical tropospheric ozone derived using Clear-Cloudy Pairs (CCP) of TOMS measurements, submitted to Journal of Atmospheric Science, 2002, hereinafter referred to as Newchurch et al., submitted manuscript, 2002]. Most products are for the tropics since the tropical stratosphere is less variable than the extratropical stratosphere and can therefore be subtracted with some confidence to yield a tropospheric residual. The TTOC products have been validated primarily with ozonesondes over the southern tropics where most tropical ozonesonde measurements are made. *Fishman et al.* [1990] found a seasonal maximum in TTOCs over the southern tropical Atlantic during September through November that they attributed to biomass burning. Further work confirmed the presence of this South Atlantic maximum and attributed it to an interplay of biomass burning, lightning, and dynamics [*Krishnamurti et al.*, 1993, 1996; *Jacob et al.*, 1996; *Pickering et al.*, 1996; *Thompson et al.*, 1996; *Moxim and Levy*, 2000]. *Martin et al.* [2000] used

empirical orthogonal functions to argue that biomass burning and lightning respectively explain 54% and 20% of the seasonal variance of TOMS TTOCs. Interannual variability is dominated by El Niño events [*Ziemke et al.*, 1998; *Thompson and Hudson*, 1999] that enhance TTOCs over Oceania due to both large-scale dynamics and increased biomass burning [*Chandra et al.*, 1998; *Thompson et al.*, 2001; *Chandra et al.*, 2002]. There is no significant long-term trend in TOMS TTOCs over 1979–1998 [*Ziemke et al.*, 1998; *Thompson and Hudson*, 1999; *Thompson et al.*, 2001].

[5] A few notable features in the distribution of TTOCs have evaded explanation. Satellite observations of fires, for example, from the Along Track Scanning Radiometer (ATSR) World Fire Atlas [*Arino and Rosaz*, 1999], show considerable biomass burning over sub-Saharan northern Africa during DJF (Figure 1). None of the TOMS TTOC products, except those of *Kim et al.* [2001] show a coincident seasonal enhancement over the region, in contrast with the seasonal enhancement seen over the southern tropical Atlantic during the austral biomass burning season from July to October. In fact, most TOMS TTOC products reach their seasonal maximum over northern Africa during the austral biomass burning season. Furthermore, the highest TTOCs during DJF are over the South Atlantic even though biomass burning in the Southern Hemisphere is then at its seasonal minimum, a result which *Thompson et al.* [2000] called the "tropical Atlantic paradox." Simulations of ozone with global tropospheric chemistry models [e.g., *Hauglustaine et al.*, 1998; *Wang et al.*, 1998b; *Lawrence et al.*, 1999; *Mickley et al.*, 1999; *Galanter et al.*, 2000; *Lelieveld and Dentener*, 2000; *Bey et al.*, 2001a] more closely track the seasonal variation in biomass burning including enhanced concentrations over northern Africa during DJF.

[6] In this paper we examine these puzzling features of the TOMS TTOCs. We explain the tropical Atlantic paradox of *Thompson et al.* [2000] and the persistent wave-1 pattern with a zonal maximum over the tropical Atlantic of approximately twice the magnitude of TTOCs over the Pacific during all seasons [*Fishman et al.*, 1990; *Ziemke et al.*, 1996, 1998; *Hudson and Thompson*, 1998; *Thompson et al.*, 2002]. We identify problems in the TTOC retrievals over northern Africa and south Asia using ozone measurements from the Measurement of Ozone and Water Vapor by Airbus In-Service Aircraft (MOZAIC) program [*Marenco et al.*, 1998]. We use radiative transfer calculations to show that the sensitivity of the TOMS retrieval to the assumed vertical profile is a contributing factor. We also show that the photochemical effects of mineral dust on ozone in the region [*Zhang et al.*, 1994; *Dentener et al.*, 1996; *De Reus et al.*, 2000] are relatively small. Finally, we use the combination of TOMS TTOCs and in situ measurements from sondes and aircraft to better constrain the global magnitude of lightning NO_x emissions, which is one of the major open questions in tropospheric chemistry [*Houghton et al.*, 2001]. Recent estimates of this source are $3-5$ Tg N yr^{-1} [*Levy et al.*, 1996], 5 (2–20) Tg N yr^{-1} [*Lee et al.*, 1997], 12 (5–20) Tg
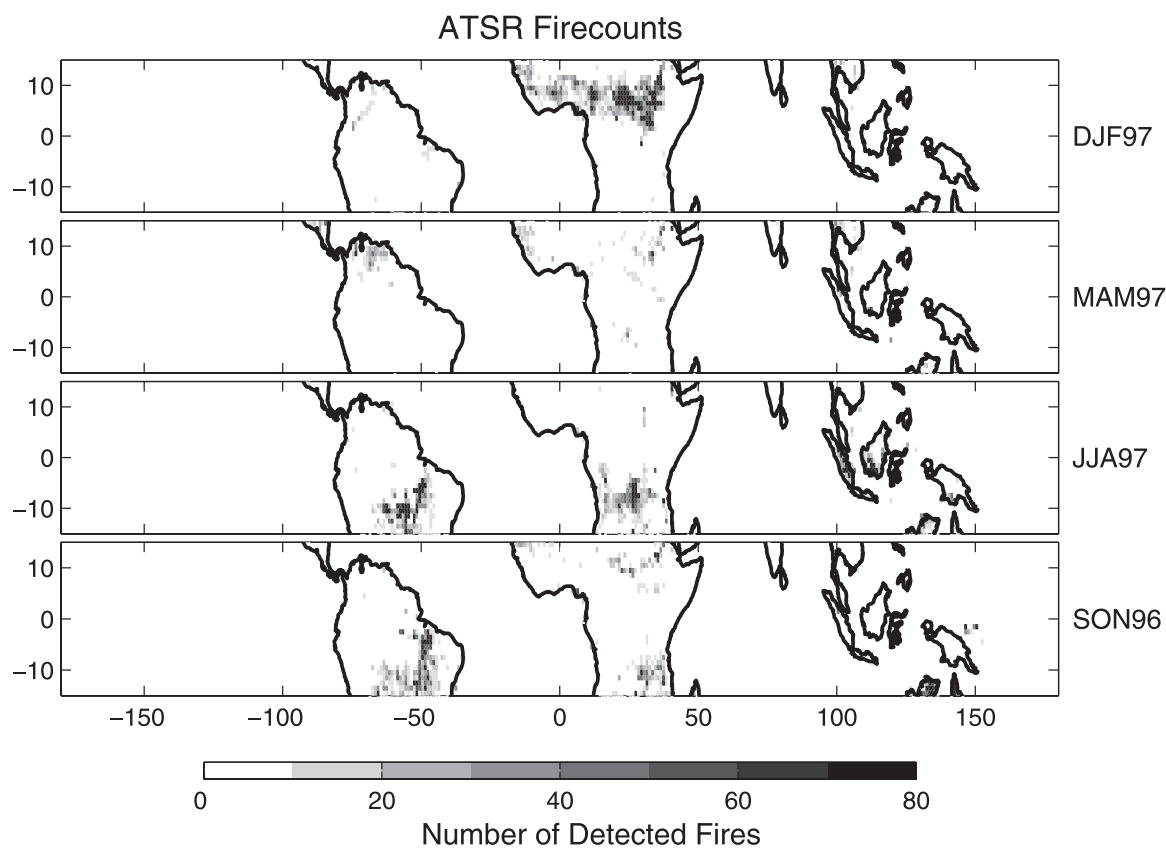
ATSR Firecounts

Figure 1.   Seasonally averaged fire-counts from the Along Track Scanning Radiometer for December 1996–February 1997 (DJF97), March 1997–May 1997 (MAM97), June 1997–August 1997 (JJA97), and September 1996–November 1996 (SON96). Data are from *Arino and Rosaz* [1999].

N yr^{-1} [*Price et al.*, 1997], 3–8 Tg N yr^{-1} [*Wang et al.*, 1998], 5 Tg N yr^{-1} [*Jourdain and Hauglustaine*, 2001], and 6 Tg N yr^{-1} [*Staudt et al.*, 2002a].

[7]   Our analysis is based on a synthesis and interpretation of TOMS and in situ measurements with the GEOS-CHEM global 3-D model of tropospheric chemistry. We focus on the period of September 1996 through August 1997 during which TTOCs are available from TOMS and are similar to the long-term mean (1979–1992; 1996–2000), biomass burning emissions can be constrained from ATSR firecounts and the TOMS Aerosol Index [*Herman et al.*, 1997; *Torres et al.*, 1998], and the large fires in Oceania associated with El Niño have not begun. Section 2 introduces the ozone data used in the analysis. Section 3 describes the GEOS-CHEM model and discusses its sensitivity to lightning NO_x emissions. In section 4 the model simulation is compared with TTOCs from TOMS. Section 5 uses aircraft observations from the MOZAIC program to resolve the disagreements between the model and TOMS over northern Africa and south Asia. Section 6 presents a correction to the TOMS tropospheric retrieval efficiency to account for ozone variability in the lower troposphere. The Atlantic paradox and wave-1 pattern in tropical tropospheric ozone are examined in section 7.

2.   Ozone Data

[8]   We focus our analysis on two techniques that have been used to produce TTOCs for the entire Nimbus 7 and EP TOMS record (1979–1992; July 1996–present). The convective cloud differential (CCD) method uses highly reflective scenes (R > 0.9) over the highly convective tropical Pacific to determine stratospheric column as a function of latitude, and assumes that these columns are zonally invariant between 15°S and 15°N [*Ziemke et al.*, 1998]. Tropospheric columns are calculated as the difference between total columns determined for low reflectivity scenes (R < 0.2) and the stratospheric column. We subtract 5 Dobson units (1 DU = 2.69×10^{20} molecules m^{-2}) from the Earth Probe TOMS CCD tropospheric columns following *Ziemke and Chandra* [1999] to account for a bias with CCD data from Nimbus 7 TOMS. The CCD method has been extended recently to a "cloud slicing" product where cloud top information is used to separate TTOCs into columns above and below 400 hPa [*Ziemke et al.*, 2001].

[9]   The modified residual method (MR) method [*Thompson and Hudson*, 1999] assumes that a wave-1 pattern in tropospheric ozone columns reaches a minimum of zero at the dateline. It uses ozonesonde data from 1991–1992 to determine the sum of the wave-1 amplitude and a zonally invariant background in tropospheric ozone. The sum is assumed to exhibit no interannual variability; the magnitude of the zonally invariant background is determined as the difference between the sum and the peak-to-peak amplitude in the tropospheric wave-1. The stratospheric column is determined from the difference between the total column and the zonally invariant tropospheric background at the dateline. Finally the method assumes a zonally invariant stratosphere to produce a tropospheric residual. It is
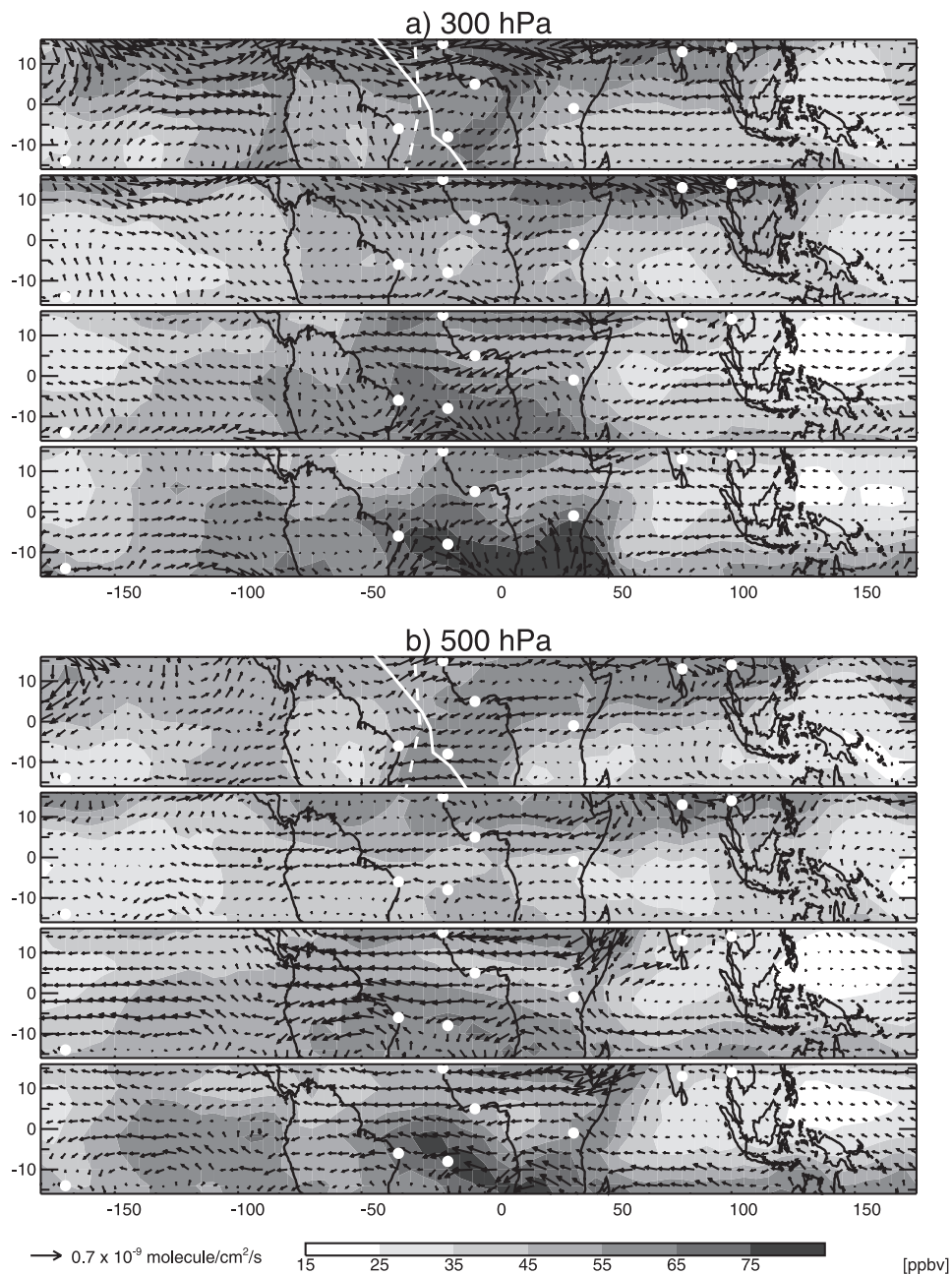
a) 300 hPa

b) 500 hPa

Figure 2. Ozone concentrations and transport fluxes calculated with the GEOS-CHEM model at (a) 300 hPa, (b) 500 hPa, and (c) 800 hPa. White circles show the locations of ozone observations from ozonesondes in the Southern Hemisphere and commercial aircraft in the Northern Hemisphere used to evaluate the model. White lines show ship tracks (Polarstern [*Weller et al.*, 1996] is dashed and Aerosols99 [*Thompson et al.*, 2000] is solid) along which ozonesondes were launched that are used here to evaluate the model. See color version of this figure at back of this issue.

restricted to latitude bands in which the wave-1 pattern dominates zonal variability for that particular month and year.

[10] Efficiency corrections have been developed for the MR method [*Hudson and Thompson*, 1998] and the CCD method [*Ziemke et al.*, 2001] in an attempt to account for lower tropospheric insensitivity and are included in the data presented here. A correction for aerosol effects on the retrieval developed by *Torres and Bhartia* [1999] is also included. The MR method filters the data for scene reflec-

tivities less than 20% to minimize cloud contamination and the CCD method accounts for clouds as described above.

[11] We also use a variety of in situ ozone observations in our analysis. Figure 2 shows the location of ozone measurement sites that we discuss in detail. Observations in the Southern Hemisphere are from four ozonesonde stations [*Logan*, 1999; *Thompson and Witte*, 1999; *Oltmans et al.*, 2002; *Thompson et al.*, 2002] discussed in section 4. Observations in the Northern Hemisphere are from the MOZAIC commercial aircraft program [*Marenco et al.*,
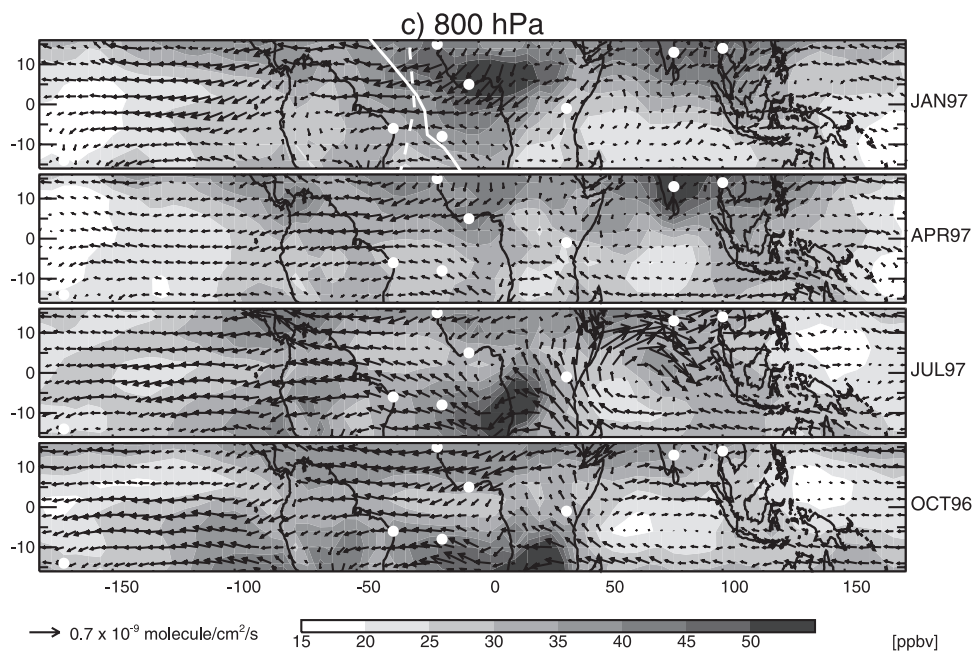
Figure 2.   (continued)

1998] and are discussed in section 5. Ozonesondes launched from ship transects across the Equator in January and February [*Weller et al.*, 1996; *Thompson et al.*, 2000] are analyzed in section 7. Figure 2 also shows simulated ozone concentrations and fluxes to which we will refer frequently.

3. GEOS-CHEM Model

3.1. Model Description

[12]   The GEOS-CHEM global 3-D tropospheric chemistry and transport model was initially described by *Bey et al.* [2001a]. We use here GEOS-CHEM version 4.11 (http://www-as.harvard.edu/chemistry/trop/geos/) with additional developments described below. The model is driven by assimilated meteorological data updated every 3–6 hours from the Goddard Earth Observing System of the NASA Data Assimilation Office (DAO) [*Schubert et al.*, 1993]. The GEOS data for 1996–1997 are available with a resolution of 2° latitude by 2.5° longitude and 46 sigma levels in the vertical extending up to 0.1 hPa. For computational expedience we degrade the horizontal resolution to 4° latitude by 5° longitude and merge the vertical levels above the lower stratosphere, retaining a total of 26 levels. We conduct simulations from March 1996 through August 1997. The first six months are used to achieve proper initialization. We present results for September 1996 through August 1997.

[13]   The GEOS-CHEM model includes a detailed description of tropospheric ozone-NO_x-hydrocarbon chemistry. It solves the chemical evolution of about 120 species with a Gear solver [*Jacobson and Turco*, 1994] and transports 24 tracers. Photolysis frequencies are computed using the Fast-J radiative transfer algorithm [*Wild et al.*, 2000] which includes Rayleigh and Mie scattering. The tropopause in the model is determined using the World Meteorological Organization standard criterion of a 2 K km^{-1} lapse rate as quoted by *Craig* [1965]. The cross-tropopause

transport of ozone is simulated by the Synoz (synthetic ozone) method [*McLinden et al.*, 2000] using their recommended flux of 475 Tg O_3 yr^{-1}.

[14]   Biogenic isoprene emissions from land are computed locally using the parameterization of *Guenther et al.* [1995], modified by *Wang et al.* [1998a] and *Bey et al.* [2001a]. Anthropogenic NO_x emissions are from the Global Emission Inventory Activity (GEIA) [*Benkovitz et al.*, 1996] and scaled to the current year as described by *Bey et al.* [2001a]. Soil NO_x emissions are computed locally using a modified version of the *Yienger and Levy* [1995] algorithm, as described by *Wang et al.* [1998a] and *Bey et al.* [2001a]. Figure 3 shows the 1996–1997 emissions of NO_x from lightning determined from cloud top height following the parameterization of *Price and Rind* [1992] as implemented by *Wang et al.* [1998a] with vertical profiles from *Pickering et al.* [1998]. Most lightning emissions are over land since the relatively weak updrafts in marine storms result in considerably fewer electrical discharges. The parameterization used here underestimates lightning emissions over marine locations, but alternative parameterizations based on convective mass flux or precipitation have the opposite problem [*Allen and Pickering*, 2002].

[15]   The model version used here includes several updates to the original version presented by *Bey et al.* [2001a]. The most important are improved biomass burning and biofuel emission inventories, doubled NO_x emissions from lightning, and accounting of scattering, absorption, and heterogeneous chemistry involving mineral dust aerosols; these are summarized below. The updated version includes also monthly-averaged UV surface reflectivity fields [*Herman et al.*, 1997], an updated isoprene oxidation mechanism described by *Fiore et al.* [2002], and scaling of the overhead ozone column used in Fast-J to the current year using monthly observations from TOMS.
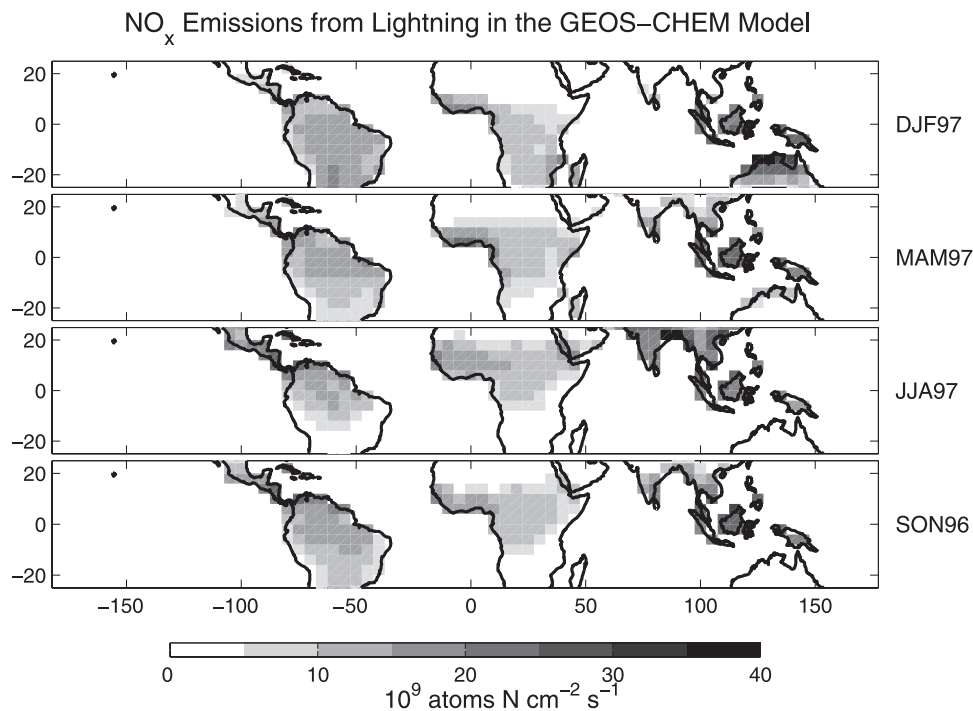
NO$_x$ Emissions from Lightning in the GEOS–CHEM Model

Figure 3. Seasonally averaged NO$_x$ emissions from lightning used in the GEOS-CHEM model, yielding a global annual source of 6 Tg N yr^{-1}.

[16] The biomass burning inventory (including deforestation, savanna burning, and wild fires) is from J. Logan and R. Yevich (personal communication, 2001) as summarized by *Lobert et al.* [1999]. Agricultural burning from R. M. Yevich and J. A. Logan (manuscript in preparation, 2002) is also included here as part of the biomass burning inventory. The biofuel emission inventory (including fuel wood, charcoal, crop residues, and dung) is from Yevich and Logan (manuscript in preparation, 2002). The most important changes relative to the older inventories used by *Bey et al.* [2001a] are increased emissions from agricultural residues in south Asia and from biofuels, in general, decreased emissions in northern Africa and Brazil, and an equatorward shift in African emissions. We use vegetation-specific emission factors for NO$_x$, CO, and different hydrocarbons as well as oxygenated organics as described by *Staudt et al.* [2002b]. Over many regions the NO$_x$/CO emission ratio from biomass burning is about half that used by *Bey et al.* [2001a]. Interannual and seasonal variation in biomass burning emissions specific to 1996–1997 are determined from the TOMS aerosol index and from ATSR fire-counts, following the method described by B. N. Duncan et al. (Interannual and seasonal variability of biomass burning emissions constrained by remotely sensed observations, submitted to the Journal of Geophysical Research, 2002).

[17] Table 1 contains the annual NO$_x$ emissions used in the updated model version. The magnitude of NO$_x$ emissions from biomass burning (5 Tg N yr^{-1}) and biofuels (2.2 Tg N yr^{-1}) is about 60% of the 12 Tg N yr^{-1} used by *Bey et al.* [2001a] for the sum of the two. The global source of 6 Tg N yr^{-1} from lightning is double that of *Bey et al.* [2001a] and is justified below. Other source formulations are identical to *Bey et al.* [2001a], but have been adjusted here to 1996–1997.

[18] Radiative and heterogeneous chemical effects of dust aerosols in the model are included as described in Appendix A, section A1. We calculate the radiative effect using a Mie algorithm [*de Rooij and van der Stap*, 1984; *Mishchenko et al.*, 1999], complex refractive indices as a function of wavelength [*Patterson et al.*, 1977], the Fast-J radiative transfer code [*Wild et al.*, 2000], and global 3-D monthly mean model fields of mineral dust from *Ginoux et al.* [2001]. We calculate heterogeneous reaction rates using a reaction probability formulation [*Ravishankara*, 1997] applied to the mineral dust concentrations of *Ginoux et al.* [2001], and with reaction probabilities recommended by *Jacob* [2000].

3.2. Model Evaluation: Sensitivity to Lightning

[19] Extensive evaluations of the GEOS-CHEM chemical fields with observations have been presented in a number of papers [*Li et al.*, 2000; *Singh et al.*, 2000; *Bey et al.*, 2001a, 2001b; *Li et al.*, 2001; *Liu et al.*, 2001; *Palmer et al.*, 2001; *Bell et al.*, 2002; *Chandra et al.*, 2002; *Fiore et al.*, 2002; *Jacob et al.*, 2002; *Li et al.*, 2002a, 2002b; *Liu et al.*, 2002;

Table 1. Global NO$_x$ Emissions for September 1996 to August 1997[a]

Source	Emission Rate, Tg N yr^{-1}
Fossil fuel combustion	23.1 (1.6)
Lightning	5.8 (3.6)
Soils	5.2 (1.9)
Biomass burning	5.1 (3.2)
Biofuels	2.2 (0.7)
Aircraft	0.5 (0.0)
Stratosphere	0.2 (0.0)[b]

[a] The values in parentheses are for the tropics (16°S–16°N).
[b] The cross-tropopause NO$_y$ flux is 0.7 Tg N yr^{-1} (including 0.2 Tg N yr^{-1} as NO$_x$ and 0.5 Tg N yr^{-1} as HNO$_3$).
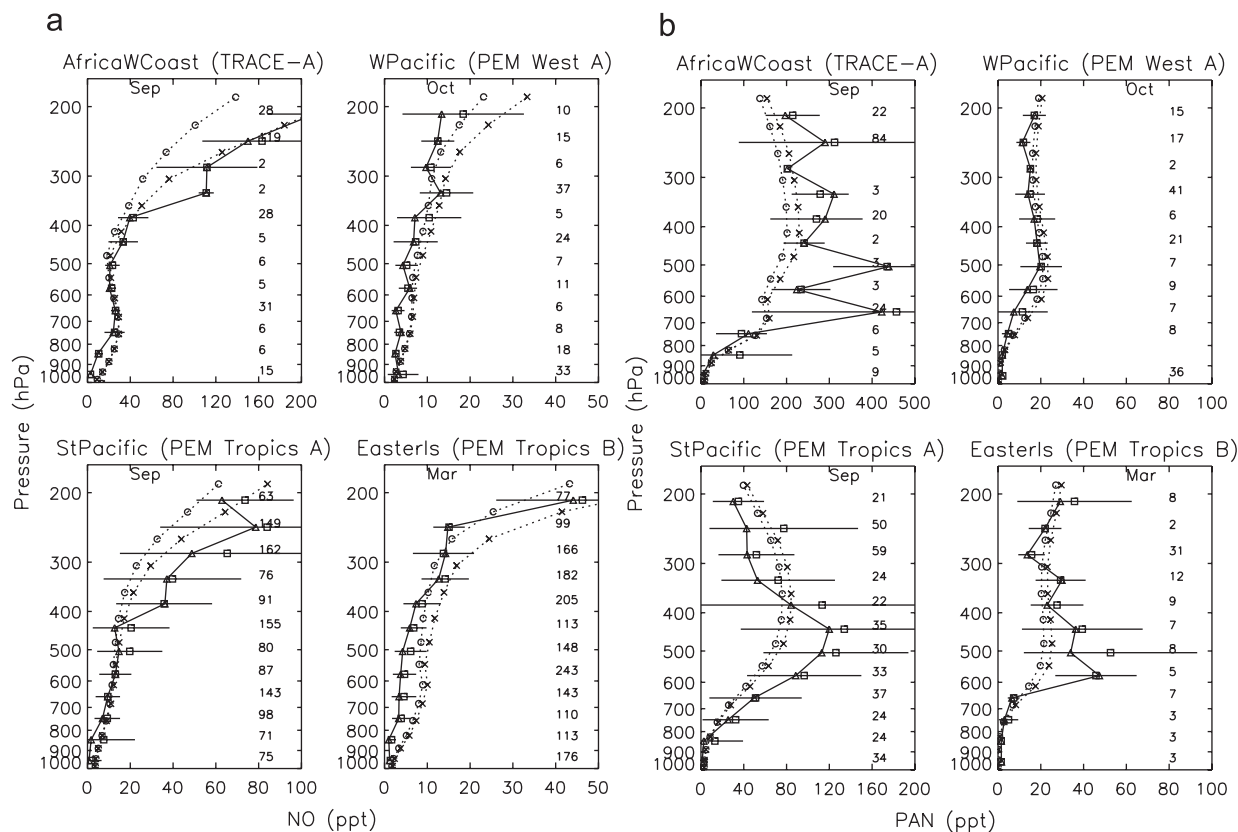
Figure 4. Comparison of aircraft observations of (a) NO and (b) PAN with the GEOS-CHEM model concentrations over the (top left) west coast of Africa during September [*Fishman et al.*, 1996]; (top right) western tropical Pacific during October [*Crawford et al.*, 1996]; (bottom left) southern tropical Pacific during September [*Hoell et al.*, 1999]; and (bottom right) Easter Island during March [*Raper et al.*, 2001]. The open squares are mean observed values (with horizontal bars for standard deviations). The open triangles and solid lines are median observed values. Dashed lines are simulated GEOS-CHEM values for September 1996–August 1997 sampled over the same region and month as the observations for the simulation with 6 Tg N yr^{-1} from lightning (crosses) and a sensitivity simulation with 3 Tg N yr^{-1} (open circles).

Martin et al., 2002; *Palmer et al.*, 2002]. Observed monthly mean ozone concentrations in different regions of the troposphere are usually reproduced to within 10 ppbv with no global bias. Observed concentrations of NO and peroxyace-tylnitrate (PAN) as well as observed columns of HCHO and NO$_2$ are generally reproduced better than a factor of 2. The tracers of convective transport ^{210}Pb, ^{7}Be, and CH$_3$I are simulated without global bias. There is a general model underestimate of CO concentrations by 10–30 ppbv [*Bey et al.*, 2001a] that is improved in a more recent model version (B. N. Duncan et al., manuscript in preparation, 2002) with revised CO emissions. We estimate that the largest potential error sources for the simulation of tropical tropospheric ozone in GEOS-CHEM are the relative spatial distribution of NO$_x$ emissions, unknown chemistry involving in particular organic and heterogeneous processes [*Jacob*, 2000; *Singh et al.*, 2001], and the simulation of convective transport.

[20] Model updates relative to *Bey et al.* [2001a] as described in section 3.1 have some implications for the simulation of tropical ozone and NO$_y$. Over the tropical Atlantic, concentrations of ozone, PAN, and NO above 500 hPa increase by about 10 ppbv, 50 pptv, and 20 pptv, respectively, largely due to the increased NO$_x$ from light-

ning. Over northern Africa during DJF, concentrations of ozone, PAN, and NO decrease by about 30 ppbv, 500 pptv, and 300 pptv, respectively in the boundary layer, largely from changes in biomass burning emissions. Effects are less over other regions.

[21] Figure 4 compares vertical profiles of NO and PAN in the tropical troposphere for simulations including either 6 Tg N yr^{-1} or 3 Tg N yr^{-1} from lightning with observations from aircraft missions for the regions presented by *Bey et al.* [2001a]. Except for PEM Tropics A, the missions were conducted in years other than the model year (September 1996–August 1997). These observations provide little constraint on the NO$_x$ source from lightning within the range of 3–6 Tg N yr^{-1}. Off the west coast of southern Africa, the simulation with 6 Tg N yr^{-1} from lightning is more consistent with observations than the one with 3 Tg N yr^{-1}. Over the Pacific, the comparison is mixed. Evaluation with observations for the other tropical and extratropical regions presented by *Bey et al.* [2001a] did not yield additional insight.

[22] We investigated whether the ozone simulation could better constrain the lightning source in view of the greater abundance of observations. Figure 5 compares the simu-
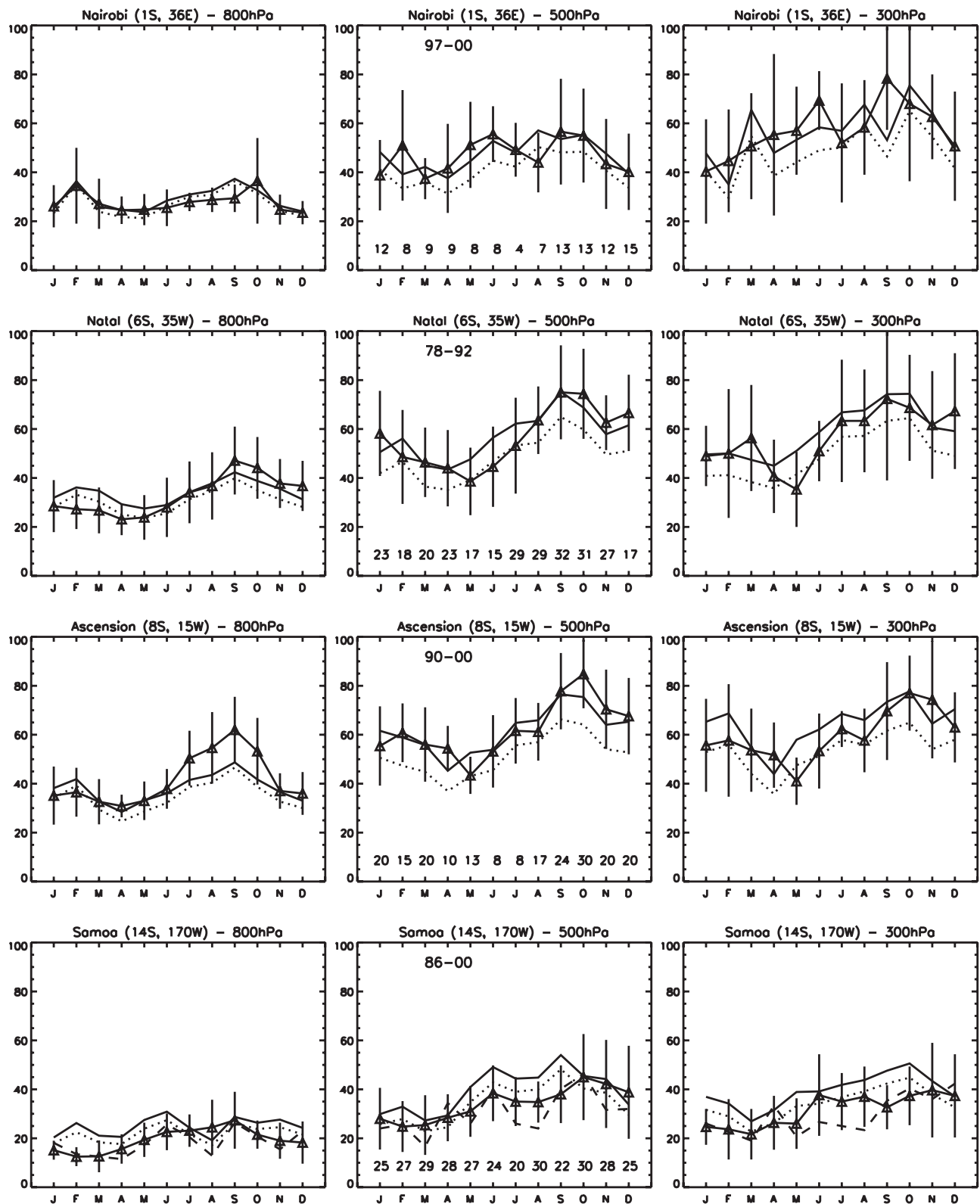
Figure 5. Seasonal variation of tropospheric ozone at tropical sites. Climatological monthly mean concentrations from ozonesonde stations (bold line with triangles) are compared to the GEOS-CHEM simulation for September 1996–August 1997 with 6 Tg N yr^{-1} from lightning (solid) and a sensitivity simulation with 3 Tg N yr^{-1} from lightning (dotted). Error bars are ±1 standard deviation. The panels in the middle column show the years over which observations were taken (top) and the number of observations for each month (bottom). The bold dashed line shows the observed seasonal variation for September 1996–August 1997 where available (Samoa).

lated seasonal variation of ozone concentrations at representative sites in the southern tropics (Figure 2). Observations for the 1996–1997 simulation period are also shown at Samoa, the only site with coincident data. The magnitude of lightning NO_x emissions has a large effect on the tropical tropospheric ozone burden in the middle and upper troposphere, especially over the tropical Atlantic sites where emissions of 6 Tg N yr^{-1} better represent observations. The simulations with 3 and 6 Tg N yr^{-1} respectively explain 78% and 81% of the variance in observed monthly mean ozone concentrations at the four sites at 100 hPa intervals throughout the troposphere (n = 480).

[23] No ozonesonde sites exist over northern Africa. The 800 hPa maximum over Nairobi in February is reproduced in the model and is due to outflow from northern African biomass burning. Ozone at higher altitudes over Nairobi peaks during the southern hemisphere biomass burning season from July through October. Figure 2 shows a southeasterly ozone flux at all three levels over Nairobi during April, July, and October. Over Natal and Ascension, the influence from biomass burning in the Southern Hemisphere is also pronounced, as had been shown previously during TRACE-A [*Thompson et al.*, 1996]. The phase of the seasonal variation in the model agrees with observations, but the amplitude is weaker than observed at low altitudes. Lightning NO_x emissions of 6 Tg N yr^{-1} in the standard simulation are important in reproducing the magnitude of the ozone observed at 500 and 300 hPa at Nairobi, Ascension, and Natal throughout most of the year. However modeled ozone is higher than observed in the upper troposphere during JJA over Ascension, Natal, and Samoa. During this season the ratio of lightning NO_x emissions in the southern tropics ($0°-15°S$) to global emissions is 30% higher when calculated with GEOS clouds than with ISCCP clouds [*Price et al.*, 1997]. *Allen et al.* [1997] found that cloud top heights in the southern tropics during JJA were overestimated in the GEOS-1 fields, an overestimate that would lead to excessive production of NO_x by lightning in our model.

[24] The model generally overestimates observations at Samoa. A similar bias exists over San Cristobal (1°S, 90°E), Tahiti (18°S, 149°W), and Fiji (18°S, 178°E). Concentrations of NO_x over the South Pacific also tend to be overestimated (Figure 3a). The discrepancy may reflect flaws in the GEOS tropical circulation [*Allen et al.*, 1997] and in the modeled spatial distribution of lightning [*Allen and Pickering*, 2002; *Staudt et al.*, 2002a]. We did not investigate the bias further.

[25] In summary, we find that simulations with either 3 or 6 Tg N yr^{-1} from lightning could represent ozonesonde observations. Evaluation at 44 other tropical and extratropical ozonesonde sites was found not to be any more conclusive. Emissions of 6 Tg N yr^{-1} from lightning better represent the Atlantic data while the Pacific data are better represented by a simulation with 3 Tg N yr^{-1} (but the model is then still somewhat high). We use 6 Tg N yr^{-1} because it results in the best simulation over the Atlantic region where ozone exhibits the highest sensitivity to lightning as will be discussed further in section 7, and because it provides a simulation most consistent with TOMS TTOCs as will be shown in section 4.

3.3. Global Budgets

[26] Table 2 shows annual mean global ozone production and loss rates for our simulations. Global chemical produc-

Table 2. Global Tropospheric Ozone Budget and CH_3CCL_3 Lifetimes[a]

	Standard[b]	Reduced Lightning[c]	No Het Chem[d]	No Dust[e]	*Bey et al.* [2001a]
Chemical production (Tg O_3 yr^{-1})	4920	4440	4630	4760	4900
Chemical loss (Tg O_3 yr^{-1})	4230	3940	4110	4230	4300
Burden (Tg O_3)	321	294	302	301	315
CH_3CCl_3 lifetime (yr)	5.3	5.9	5.7	5.4	5.1
Mean TTOC[f] (DU)	29.6	26.0	26.6	26.4	

[a]The production, loss, and burden are actually for the extended odd oxygen family defined as $O_3 + NO_2 + 2*NO_3 + $ peroxyacylnitrates $+ HNO_3 + 3*N_2O_5$. They are calculated for the column extending to the local model tropopause. The CH_3CCl_3 lifetime is calculated as the ratio of the total burden of atmospheric CH_3CCl_3 to the tropospheric loss rate against oxidation by OH [*Spivakovsky et al.*, 2000]. Values are annual means for September 1996 to August 1997 from the GEOS-CHEM model.
[b]The standard simulation includes the photochemical effects of mineral dust, and 6 Tg N yr^{-1} from lightning.
[c]Same as standard simulation but with 3 Tg N yr^{-1} from lightning.
[d]Same as standard simulation but with 3 Tg N yr^{-1} from lightning and no heterogeneous chemical effects of mineral dust.
[e]Same as standard simulation but with 3 Tg N yr^{-1} from lightning and no radiative or chemical effects of dust.
[f]For the $16°S–16°N$ latitude range.

tion, loss, and tropospheric ozone burden for our standard simulation are within 2% of the values given by the *Bey et al.* [2001a] simulation which had higher biomass burning emissions of NO_x (12 Tg N yr^{-1}), lower emissions from lightning (3 Tg N yr^{-1}) and biofuels, and did not account for the radiative and heterogeneous chemical effects of dust. As seen in Table 2, the combination of these changes cancels in the global ozone budget. The resulting global CH_3CCl_3 lifetime of 5.3 years against oxidation by tropospheric OH is 0.2 years longer than in the simulation by *Bey et al.* [2001a], and is within the uncertainty of estimates from observations of 5.7 ± 0.7 years [*Spivakovsky et al.*, 2000] and 6.0 (+1.0, −0.7) years [*Prinn et al.*, 2001].

4. Comparison of GEOS-CHEM and TOMS TTOCs

[27] Figure 6 compares GEOS-CHEM model results for September 1996 through August 1997 with the global distribution of TTOCs from the MR and CCD methods. Data from the MR method are shown for latitudes $10°S–10°N$ because of limited data availability at higher latitudes. The model reproduces the persistent zonal maximum over the tropical Atlantic seen in TOMS TTOCs with a seasonal maximum in SON and a seasonal minimum during MAM. It also reproduces the persistent zonal minima observed in TOMS TTOCs east of Oceania. Modeled TTOCs show enhancements from biomass burning over northern Africa during DJF and south Asia during MAM, features not observed by the TOMS CCD and MR methods. A recent direct tropospheric ozone retrieval of TOMS data based on scan angle does reveal TTOC enhancements over northern Africa during DJF [*Kim et al.*, 2001].

[28] The comparison between GEOS-CHEM and TOMS TTOCs warrants some clarification of the tropical tropopause. Recently it has become clear that the top of the Hadley circulation occurs near 14–15 km, above which there is little convective outflow; air that detrains above this
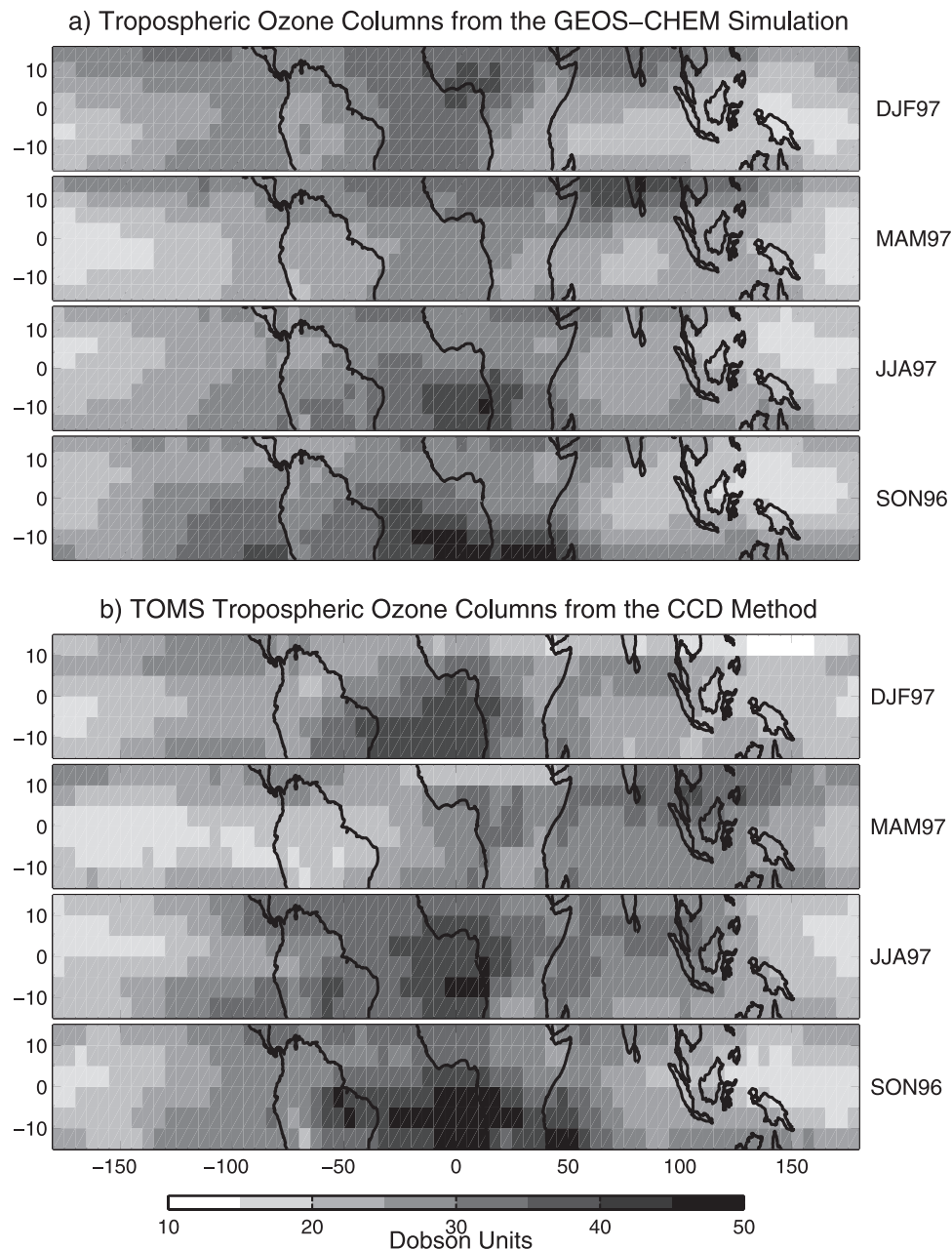
a) Tropospheric Ozone Columns from the GEOS–CHEM Simulation

b) TOMS Tropospheric Ozone Columns from the CCD Method

Figure 6. Seasonally averaged tropical tropospheric ozone columns (TTOCs) from TOMS for (a) the standard GEOS-CHEM simulation for September 1996–August 1997, (b) the convective cloud differential (CCD) method for September 1996–August 1997 [*Ziemke et al.*, 1998] including the efficiency correction described by *Ziemke et al.* [2001], and (c) The modified residual (MR) method for 1979–1992 [*Thompson and Hudson*, 1999]. See color version of this figure at back of this issue.

level either mixes with the extratropical stratosphere or slowly rises to the thermal tropopause at 16–17 km and into the tropical stratosphere [*Highwood and Hoskins*, 1998; *Folkins et al.*, 1999]. Here we refer to the tropopause as the thermal tropopause, and TTOCs as ozone columns below the thermal tropopause as derived from the CCD and MR methods and also from the GEOS-CHEM model.

[29] Table 3 gives biases and correlation statistics for GEOS-CHEM versus TOMS TTOCs in the tropics (15°S–15°N). The standard simulation has no significant global bias with TOMS TTOCs, but the simulation with reduced lightning emissions is 8–15% too low. The correlation

reflects both the spatial and temporal variation. The model captures 44% of the variance in monthly mean CCD TTOCs, a result that is not significantly altered when lightning NO_x emissions are reduced or dust effects are suppressed. The relationship with climatological CCD TTOCs over a restricted latitudinal band (10°S–10°N) is presented for comparison with climatological MR TTOCs. Over this restricted region, GEOS-CHEM explains more variance in CCD TTOCs (56%) than MR TTOCs (41%).

[30] The changes in TTOCs due to the combined radiative and chemical effects of mineral dust are shown in Figure 7. We find that mineral dust causes a decrease in
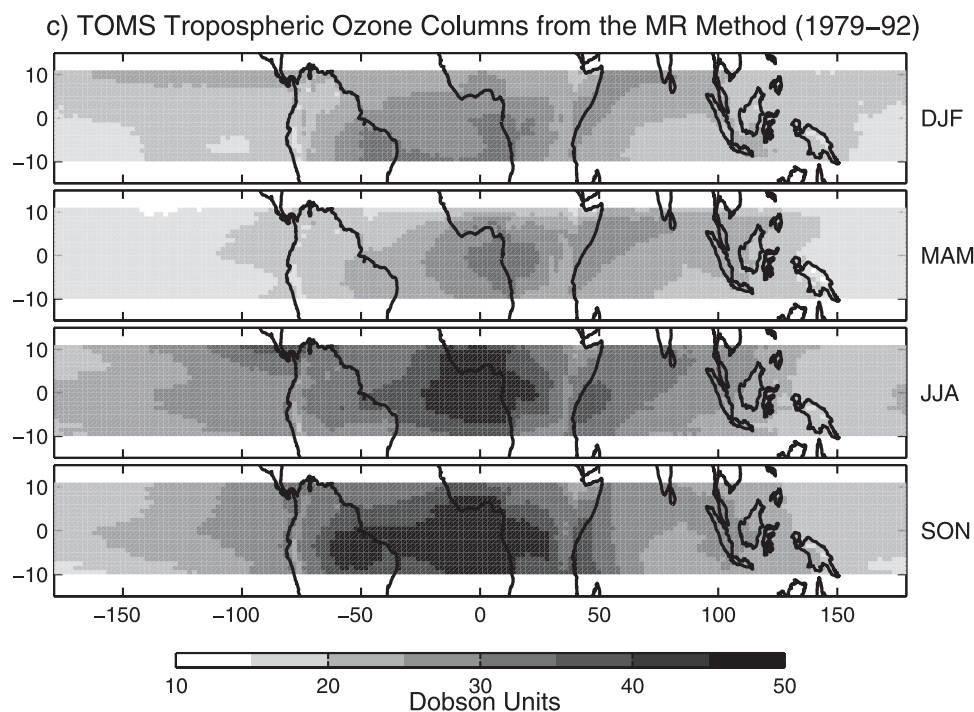
c) TOMS Tropospheric Ozone Columns from the MR Method (1979–92)

Figure 6. (continued)

ozone but the effect is small everywhere (<1.5 DU) due to competing factors as described in section A2. Biomass burning aerosol concentrations are generally lower than those from mineral dust [*Chin et al.*, 2002]. Their effect is the subject of further work.

[31] Figure 8 shows the spatial variability in the temporal correlation of monthly mean TTOCs (n = 12) between GEOS-CHEM and TOMS. Over much of the southern tropics TTOCs have been validated extensively using ozonesonde data [*Hudson and Thompson*, 1998; *Ziemke et al.*, 1998; *Thompson and Hudson*, 1999; *Ziemke and Chandra*, 1999; *Ziemke et al.*, 2001; *Chandra et al.*, 2002; *Thompson et al.*, 2002]. The temporal correlation between GEOS-CHEM and CCD TTOCs is high over much of this region, approaching 0.95 over southeastern Africa. In contrast, the northern African and Atlantic regions exhibit the weakest temporal correlation and negative values are found over an extended region, indicating that the seasonal cycle is out of phase. Over the longer record (1979–1992) the disagreement is less pronounced, but GEOS-CHEM TTOCs are not

significantly correlated with CCD and MR TTOCs over much of northern Africa and the northern tropical Atlantic. The weak correlation between GEOS-CHEM TTOCs (Sep96–Aug97) and long-term mean TOMS TTOCs (79–92) over southern Oceania is due to interannual variability. The development of the 1997–1998 El Niño and associated changes in ozone from both biomass burning and dynamics [*Chandra et al.*, 1998; *Thompson et al.*, 2001; *Chandra et al.*, 2002] are captured well by the GEOS-CHEM model [*Chandra et al.*, 2002], but are not apparent in long-term mean TTOCs. The correlation between GEOS-CHEM and MR TTOCs is generally not significant, exhibiting a broad region of negative correlation over the Indian Ocean, northern Africa, and the northern tropical Atlantic.

5. Ozone Over Northern Africa and South Asia

[32] The largest discrepancies between GEOS-CHEM and TOMS TTOCs occur over the northern tropics, including in particular northern Africa and to a lesser degree south

Table 3. Comparison Between TOMS and GEOS-CHEM TTOCs[a]

TOMS Product	GEOS-CHEM Standard		GEOS-CHEM Reduced Lightning[b]	
	Bias, DU	r	Bias, DU	r
CCD (Sep96–Aug97)	−0.5	0.66	−4.1	0.64
Corrected[c] CCD (Sep96–Aug97)	0.4	0.76	−3.1	0.75
CCD[d] (79–92)	1.3	0.75	−2.3	0.74
MR[d] (79–92)	−0.9	0.64	−4.4	0.60

[a] Bias calculations are performed between GEOS-CHEM TTOCs averaged over the period September 1996 through August 1997 and TOMS TTOCs averaged over the time periods indicated in the table. Correlations are calculated from monthly mean TTOCs at $5° \times 5°$ resolution (n = 5184 over 15°S–15°N).

[b] Global source of 3 Tg N yr^{-1}, as compared to 6 Tg N yr^{-1} in the standard simulation.

[c] CCD method corrected as discussed in section 6 for departure of the vertical ozone profile from the standard profile assumed in the TOMS retrievals.
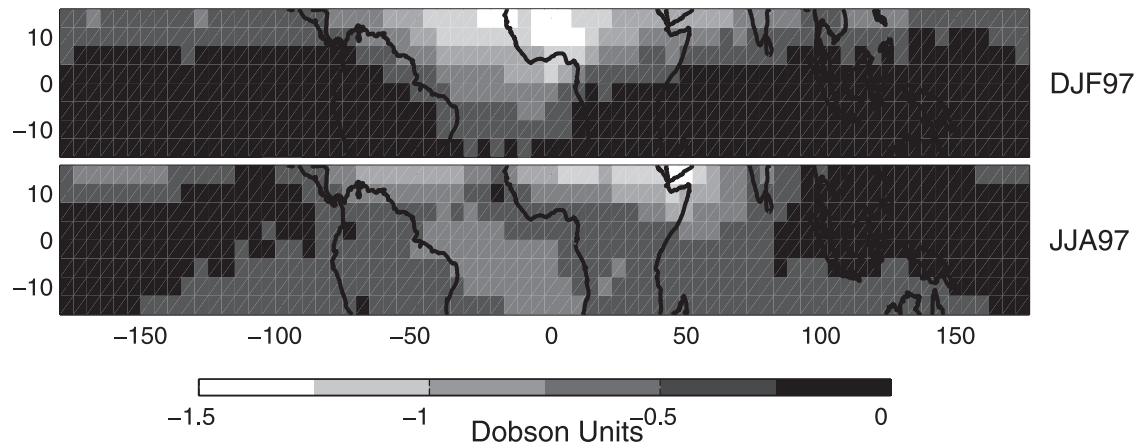
[d] Over 10°S–10°N (n = 3456).

Figure 7. Seasonally averaged change in simulated TTOCs due to the radiative and chemical effects of mineral dust for DJF97 and JJA97, as determined by difference between the standard simulation and a simulation without dust.

Asia. We examine these regions in more detail using ozone profiles measured by commercial aircraft as part of the MOZAIC program [*Marenco et al.*, 1998].

5.1. Northern Africa

[33] Figure 9 (top) compares monthly mean ozone profiles over Abidjan (5.5°N, 4°W) calculated using the GEOS-CHEM model with profiles measured from commercial aircraft during 1997 through 2000. Observations show that during the DJF biomass burning season, ozone

near 800 hPa is enhanced by up to 50 ppbv with respect to the rest of the year. The model exhibits similarly enhanced lower tropospheric values, although it does not capture adequately the sharp gradient between ozone-depleted air in the surface monsoonal flow and ozone-enhanced air from biomass burning outflow being transported near 800 hPa by northeasterly winds (Figure 2c) [*Marenco et al.*, 1990; *Andreae et al.*, 1992; *Fontan et al.*, 1992]. Both modeled and measured ozone are generally higher during DJF than the rest of the year, exhibiting no influence from

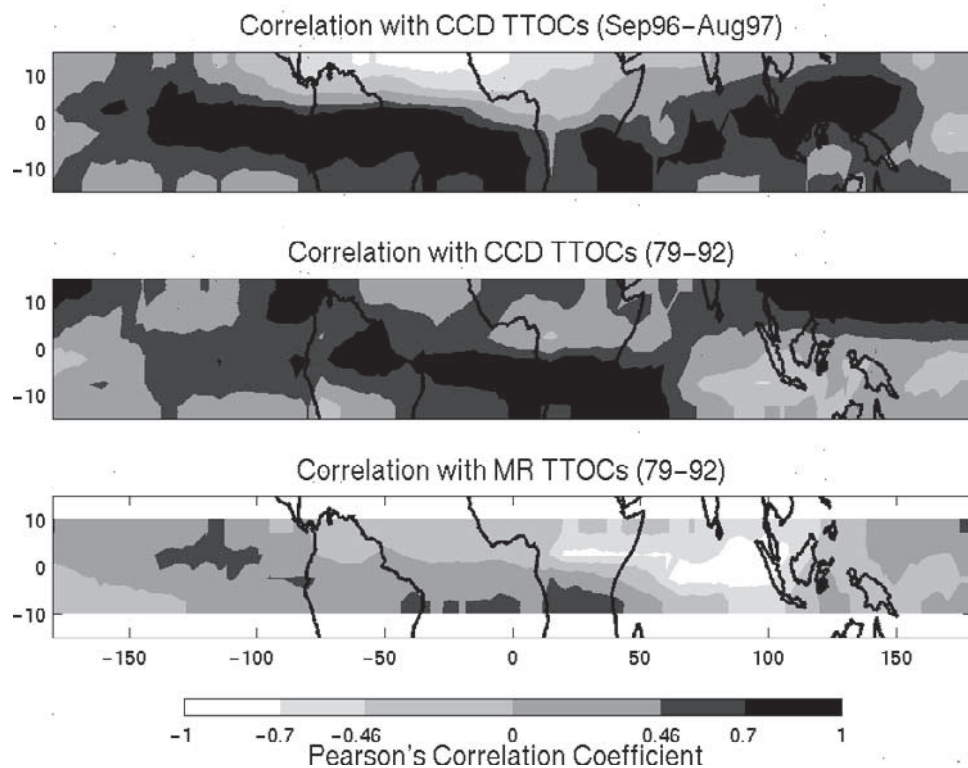**Figure 8.** Temporal correlation (**r**) between the GEOS-CHEM standard simulation (September 1996– August 1997) and TOMS TTOCs. Values greater than 0.46 and 0.7 are statistically significant at the 0.05 and 0.0025 levels, respectively (n = 12).
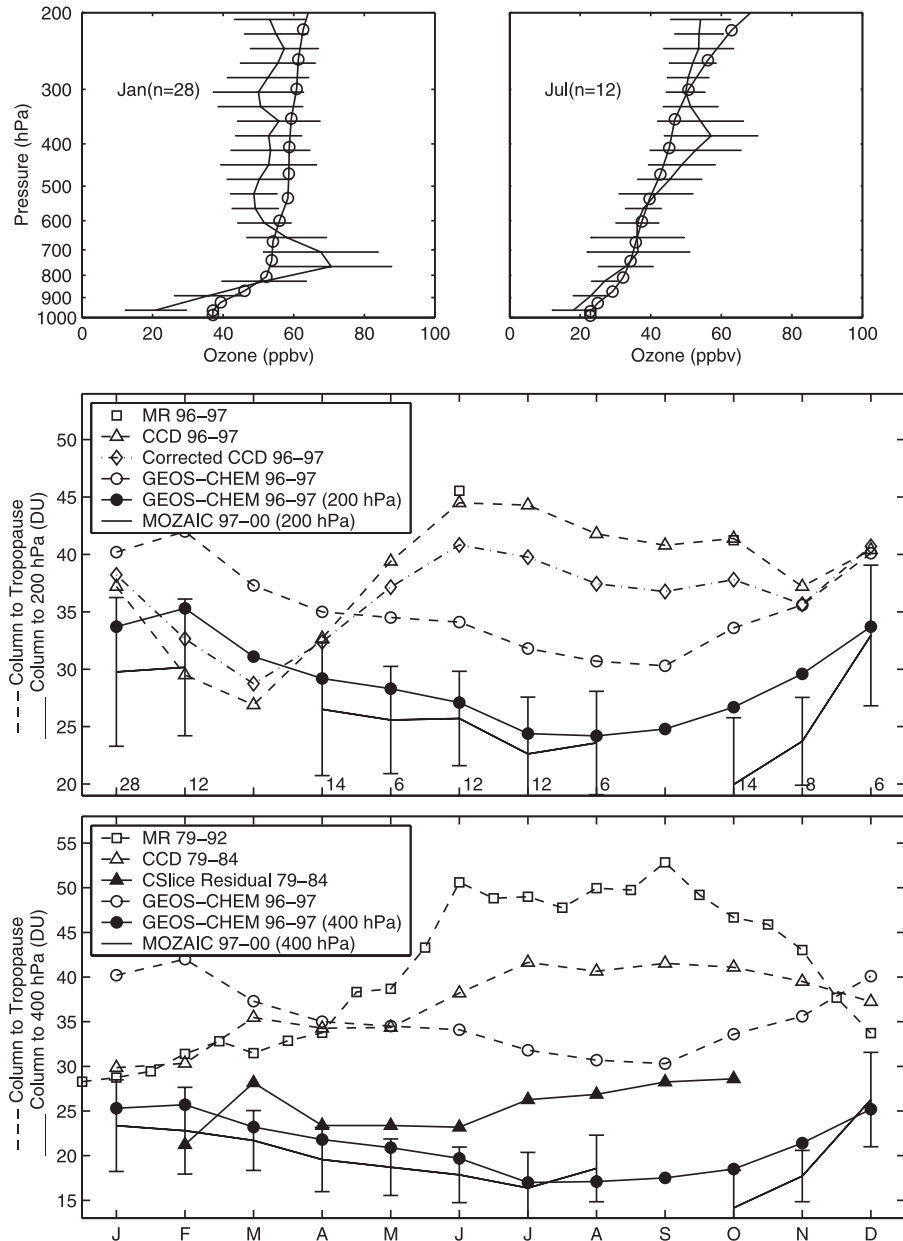
Figure 9. Tropospheric ozone over Abidjan (5°N, 4°W). The top panels show monthly mean vertical profiles in January and July. Lines with error bars are measurements from MOZAIC. Error bars indicate standard deviations. The number of observations for each month is in parentheses. Lines with circles are standard model results. The middle panel shows the seasonal variation of TTOCs extending up to the tropopause (dashed and open symbols) and columns below 200 hPa (solid and filled symbols) calculated from the MR method, the CCD method including the efficiency correction described by *Ziemke et al.* [2001], in situ measurements (MOZAIC), the GEOS-CHEM model, and CCD columns corrected for the Rayleigh scattering induced reduction in TOMS sensitivity to lower and middle tropospheric ozone as described in section 6. The number of MOZAIC vertical profiles contributing to the monthly mean column is shown at the bottom of the panel. The bottom panel shows TTOCs (dashed) and columns below 400 hPa (solid) above Abidjan calculated from the MR method, the CCD method, the residual between CCD TTOCs and cloud slicing [*Ziemke et al.*, 2001], MOZAIC, and the GEOS-CHEM model.

the southern hemisphere biomass burning season during July through October.

[34] Figure 9 (middle) shows the seasonal variation in the total tropospheric column and the ozone column below 200 hPa over Abidjan. The commercial aircraft used in MOZAIC have a ceiling of ~200 hPa. We calculate

columns from MOZAIC data using all available observations at each pressure level. We show the GEOS-CHEM model columns extending up to both 200 hPa and the tropopause to facilitate comparison between MOZAIC data and TOMS TTOCs. We find that the simulated seasonal variation in the ozone column below 200 hPa is consistent

with MOZAIC measurements. Tropospheric columns calculated up to the model tropopause exhibit similar seasonal variation as those calculated up to 200 hPa. In contrast, the seasonal variations in ozone columns from the CCD method are out of phase with both the MOZAIC data and the model results. Only two observations are available from the MR method over Abidjan for September 1996 through August 1997; they agree with the CCD method and are similarly inconsistent with the MOZAIC observations and the model.

[35] Figure 9 (bottom) provides an additional perspective that directly compares MOZAIC data with TOMS ozone columns below 400 hPa by subtracting cloud slicing data available for 1979–1984 [*Ziemke et al.*, 2001] from the CCD TTOCs. By placing this comparison in the context of the difference between the GEOS-CHEM and CCD TTOCs, also shown on the bottom panel, it appears that most of the TOMS anomaly is driven by low altitudes (below 400 hPa). The multiyear mean tropospheric ozone columns from TOMS also show the temporal persistence of the seasonal variation in both the CCD and MR methods.

[36] We similarly compared modeled and TOMS TTOCs with MOZAIC observations (not shown) over Dakar (14.5°N, 17.5°W), a location north of the biomass burning region. Again the model profiles are consistent with in situ observations, although the model is biased high. Ozone columns from the CCD and MR products over Dakar exhibit a seasonal variation with a broad maximum from June–October that is inconsistent with the relatively flat seasonal variation determined from in situ observations and the GEOS-CHEM model.

5.2. South Asia

[37] Ozone measurements off the southwest coast of India during the Indian Ocean Experiment (INDOEX) in February and March 1999 revealed enhanced (>50 ppbv) ozone in the lower troposphere that has been attributed to biomass burning and anthropogenic activity [*Lal and Lawrence*, 2001; *Lelieveld et al.*, 2001]. The GEOS-CHEM ozone fields at 800 hPa exhibit a similar enhancement (Figure 2c). Figure 10 (top) compares the GEOS-CHEM monthly mean ozone profiles with MOZAIC observations at Bangkok (14°N, 101°E). Both the model and observations indicate lower tropospheric ozone values of greater than 50 ppbv during February. No such enhancement exists during September, with observations and the model indicating lower tropospheric values of less than 20 and 35 ppbv respectively. The model overestimates ozone in the free troposphere during February and in the lower troposphere during September.

[38] The middle and bottom panels of Figure 10 show the seasonal variation in the tropospheric ozone column as in Figure 9 for Abidjan. The seasonal variation is driven by the Asian monsoon and biomass burning [*Pochanart et al.*, 2000; *Liu et al.*, 2002]. In both cases the model seasonal variation is consistent with the MOZAIC aircraft observations, despite a model overestimate of about 10 DU. In contrast, the seasonal variation reported by the MR, CCD, and cloud slicing products residual products are inconsistent with the seasonal variation reported by MOZAIC. The seasonal variation in the cloud slicing product above 400 hPa (open triangles minus solid triangles) appears consistent with MOZAIC column, implying that the discrepancy

between TOMS and MOZAIC is driven by the column below 400 hPa.

[39] We find similar agreement in the column seasonal variation between the GEOS-CHEM model and MOZAIC observations over the coastal city of Madras (13°N, 80°E), both of which are out of phase with the seasonal variation retrieved from TOMS (not shown). Model ozone values in the boundary layer however, are 20 to 30 ppbv higher than observations throughout the year. *Lal and Lawrence* [2001] found a model overestimate of comparable magnitude during February and March at Ahmedabad (23°N, 73°E) and Trivandrum (8.6°N, 77°E); an overestimate they speculate arises from ozone titration by NO_x in the urban plume, difficulty resolving coastal dynamics, and heterogeneous aerosol chemistry not represented in the model. Larger scale processes may also play a role. Ozonesonde measurements taken over the Maldives at Kaashidhoo (5°N, 74°E) [*Thompson et al.*, 2002] are 10–15 ppbv higher than GEOS-CHEM model values in the lower troposphere during February 1999 and 20–30 ppbv higher in the free troposphere during March 1999. Models have difficulty resolving ozone depletion associated with the monsoon [*Law et al.*, 2000]. Observations of NO_2 from the Global Ozone Monitoring Experiment (GOME) instrument suggest that NO_x emission inventories could be too high in India [*Martin et al.*, 2002].

6. Correction to TOMS Retrieval in the Lower Troposphere

[40] The TOMS TTOCs from the CCD and MR methods have been validated previously by comparison with ozonesondes, mainly in the southern tropics [*Hudson and Thompson*, 1998; *Ziemke et al.*, 1998; *Thompson and Hudson*, 1999; *Ziemke and Chandra*, 1999; *Ziemke et al.*, 2001; *Chandra et al.*, 2002; *Thompson et al.*, 2002]. In contrast to the southern tropics, the seasonal variation in the northern tropics appears driven largely by the lower troposphere (Figures 9 and 10). The discrepancy between TOMS TTOCs and the MOZAIC observations in the northern tropics (section 5) suggests that the TOMS products underestimate the observed column when lower tropospheric ozone is high, and overestimate the column when lower tropospheric ozone is low. The sensitivity of the TOMS instrument to the lower troposphere is poor due to low surface albedos over nonfrozen surfaces and strong Rayleigh scattering; therefore the TOMS algorithm has limited tropospheric information from the instrument and is biased by the assumption of standard tropical tropospheric ozone profiles [*Klenk et al.*, 1982; *Hudson et al.*, 1995; *Wellemeyer et al.*, 1997; *McPeters et al.*, 1998; *Kim et al.*, 2001]. Here we develop a correction for the insensitivity of TOMS to lower tropospheric ozone.

6.1. Development of the Efficiency Correction

[41] Figure 11 (left) shows the sensitivity of the TOMS instrument to ozone mixing ratio that we calculate for a typical case with the Linearized Discrete Ordinate Radiative Transfer (LIDORT) model [*Spurr et al.*, 2001]. Previous similar applications of LIDORT to air mass factor (AMF) calculations for satellite retrievals are presented by *Palmer et al.* [2001] and *Martin et al.* [2002]. The TOMS instru-
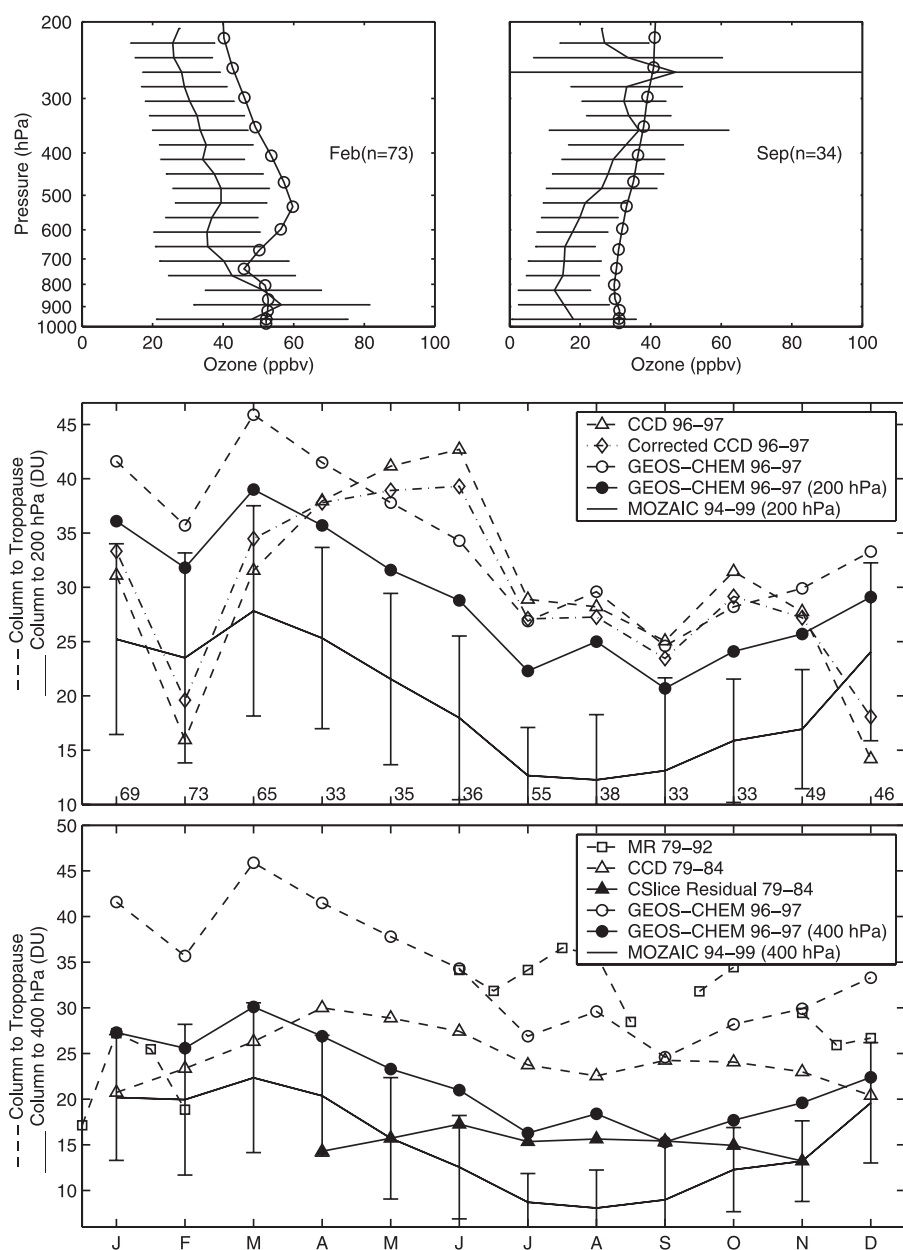
Figure 10. As in Figure 9, but for Bangkok (14°N, 101°E).

ment has less than 20% sensitivity to an increment in ozone mixing ratio near the surface, as compared to 100% at 300 hPa. Thus the TTOCs reported by TOMS will respond with only 20% sensitivity to a deviation from the assumed standard profile near the surface. Above 300 hPa, the sensitivity is slightly greater than 1 due to multiple scattering. The dotted lines in Figure 11 (right) show the three standard tropospheric ozone profiles used in the TOMS retrieval algorithm for all locations and seasons in the tropics [*McPeters et al.*, 1998]. They are nearly identical below 300 hPa.

[42] Efficiency corrections have been developed for the MR method [*Hudson and Thompson*, 1998] and the CCD method [*Ziemke et al.*, 2001] to account for the insensitivity to lower tropospheric ozone. The corrections are based on the assumption of a linear relationship between the total ozone column and the lower tropospheric column. The CCD efficiency correction scales the observed total column by the difference between it and the ~35 DU ozone column in the assumed ozone profile, assuming a 50% retrieval efficiency below 500 hPa [*Ziemke et al.*, 2001]. It is unclear what value of the retrieval efficiency is assumed in the MR method [*Hudson and Thompson*, 1998; *Thompson and Hudson*, 1999]. The observed ozone profiles in Figure 11 (right) show the weakness in assuming a linear relationship between the total tropospheric and lower tropospheric ozone columns. The ozone profile over the southern tropical Atlantic exhibits enhanced upper tropospheric ozone to which TOMS is sensitive, but no corresponding lower tropospheric enhancement [*Thompson et al.*, 2000]. In contrast, the ozone profile over Abidjan shows enhanced lower tropospheric air that is not accompanied by a corresponding upper tropospheric ozone enhancement [*Marenco et al.*, 1998].
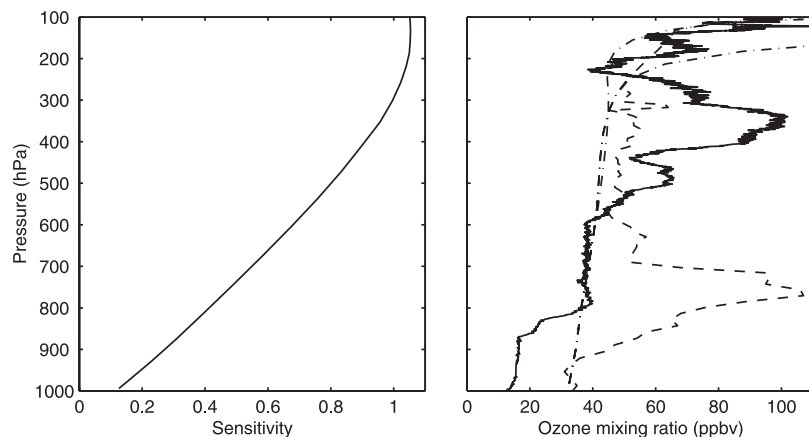
Figure 11. The left panel shows the sensitivity of the TOMS retrieval algorithm to deviations from the standard ozone profile in a Rayleigh scattering atmosphere, calculated for a representative case (nadir viewing instrument, solar zenith angle = 30°, surface albedo = 5%, wavelength = 317 nm). The right panel compares the three standard tropical ozone profiles used in the TOMS retrieval algorithm (dashed-dotted lines) with sample ozone profiles observed in January over the southern tropical Atlantic (solid line; 11°S, 10°W) [*Thompson et al.*, 2000] and Abidjan (5°N, 4°W; dashed line) [*Marenco et al.*, 1998].

[43] Here we examine how the assumption of a standard ozone profile in the TOMS retrieval algorithm affects the discrepancy between in situ and TOMS measurements. Using vertical ozone profiles from the GEOS-CHEM model in order to have global coverage, we determine a column efficiency correction $\Delta\Omega$ by integrating the difference between the modeled ozone mixing ratio c_M and the assumed TOMS mixing ratio from the standard profile c_A, weighted by the TOMS instrument sensitivity ε (Figure 11) as a function of pressure p

$$\Delta\Omega = \alpha \int_{P_S}^{P_T} (1-\varepsilon)(c_M - c_A)dp, \qquad (1)$$

where $\alpha = 7.9 \times 10^5$ DU hPa^{-1} is a unit conversion factor. The integral is calculated from the surface P_S to P_T = 300 hPa above which the instrument sensitivity approaches 1.

[44] The TOMS instrument sensitivity ε is a function of surface albedo, surface pressure, and the effective solar zenith angle θ_E (sec θ_E = secθ_o + secθ − 1) [*Palmer et al.*, 2001], where θ is the satellite zenith viewing angle and θ_o is the solar zenith angle. We use the LIDORT model to calculate its global distribution at a monthly resolution using local surface pressures from the GEOS-CHEM model and local surface albedos from *Herman and Celarier* [1997]. Surface albedos are typically 2–4% over land and 6–8% over ocean [*Herman and Celarier*, 1997] yielding a corresponding variation in ε of a few percent. We use a typical θ_E of 30° for TOMS over the tropics. We use the 275 DU standard ozone profile [*McPeters et al.*, 1998] to specify $c_A(p)$. Calculations for the 225 DU and 325 DU standard ozone profiles do not yield significantly different results.

6.2. Application

[45] Figure 12 illustrates the spatial distribution of the efficiency correction. Over biomass burning regions with enhanced lower tropospheric ozone, the TOMS retrieval

algorithm underestimates the ozone column by 3–5 DU. Over oceanic regions with ozone-depleted air, the TOMS retrieval algorithm overestimates the ozone column by 2–5 DU; the largest overestimate occurs over the western Pacific where surface ozone concentrations are typically less than 20 ppbv (Figure 2c) [*Piotrowicz et al.*, 1991; *Oltmans et al.*, 1998]. Efficiency corrections calculated from the simulation with reduced lightning emissions do not differ significantly from the values presented here.

[46] The distribution of the efficiency correction (Figure 12) is significantly correlated ($\mathbf{r}$ = 0.89, n = 5184, p < 0.0005) with the distribution of GEOS-CHEM TTOCs (Figure 6). Since the efficiency correction largely reflects the abundance of ozone in the lower troposphere, the similarity supports the correlation between total column ozone and lower tropospheric column ozone assumed by *Hudson and Thompson* [1998] and *Ziemke et al.* [2001]. The latitudinal gradient in TTOCs during DJF over the tropical Atlantic is an important exception. During this time a lower tropospheric enhancement over the northern tropical Atlantic from African outflow is unaccompanied by a corresponding upper tropospheric enhancement, and an upper tropospheric enhancement over the southern tropical Atlantic is unaccompanied by a corresponding lower tropospheric enhancement (Figure 2a versus Figure 2c) [*Weller et al.*, 1996; *Thompson et al.*, 2000].

[47] The efficiency correction algorithm presented here can be applied to any TOMS retrieval that uses the standard ozone tropical profiles. We apply it to TTOCs from the CCD method since they are also available without any previous tropospheric efficiency correction. Figure 13 shows the resulting distribution in CCD TTOCs, reflecting both the removal of the efficiency correction developed by *Ziemke et al.* [2001] from the distribution shown in Figure 8, and adding the correction developed here. The bias between corrected CCD and the GEOS-CHEM TTOCs shifts from −0.5 DU to 0.4 DU, and the correlation coefficient improves from $\mathbf{r}$ = 0.66 to $\mathbf{r}$ = 0.76 (Table 3). The higher correlation reflects in part the correlation

Correction for TOMS Retrieval Efficiency

Figure 12. Seasonally averaged efficiency correction $\Delta\Omega$ (DU) to the TOMS tropospheric ozone column retrievals to account for the insensitivity of the instrument to ozone in the lower troposphere (section 6). See color version of this figure at back of this issue.

between the efficiency correction and the GEOS-CHEM fields. In the corrected CCD fields, the latitudinal gradient in TTOCs during DJF over the tropical Atlantic decreases from almost 20 DU (Figure 6b) to 10 DU (Figure 13). The magnitude of TTOCs over northern Africa during JJA and SON decreases by about 5 DU.

[48] The middle panels of Figures 9 and 10 show that the efficiency correction improves the agreement between CCD TTOCs and observations over both Abidjan and Bangkok but is insufficient to explain the discrepancy. The behavior at Dakar and Madras is similar. At the ozonesonde locations of Nairobi, Samoa, Natal, and Ascension, the efficiency correction generally has little effect on the agreement between CCD TTOCs and observations; the ozone profiles at these locations are generally similar to the standard ozone profile assumed in the TOMS algorithm.

[49] Although it is tempting to suggest that the influence of mineral dust or soot on the TOMS retrieval could explain the remaining discrepancy of TTOCs from TOMS with both models and in situ observations over northern Africa, we do not believe this to be the case. The spatial extent of the disagreement between TOMS TTOCs and GEOS-CHEM TTOCs (Figure 8) does not match the spatial extent of mineral dust (Figure A1). The largest discrepancies between TOMS and in situ observations over Abidjan and Dakar are during July–October when there is a large dust column over Dakar but little aerosol from mineral dust or soot over Abidjan [Herman et al., 1997; Chin et al., 2002]. Mineral dust concentrations are low over Madras and Bangkok.

[50] Zonal variation in tropopause pressures, in contrast to the zonal homogeneity assumed by the CCD algorithm, does not appear to explain the discrepancy either. The GEOS fields and radiosondes [Seidel et al., 2001] show that tropopause pressures are lower over the northern tropical Pacific than over northern Africa and south Asia during December through March. Therefore the determination of the stratospheric ozone column over the Pacific and the subsequent assumption of zonally invariant stratospheric columns in the CCD and MR methods could contribute to an overestimate of the stratospheric column over northern Africa and south Asia. The resulting TTOC overestimate is about 1 DU for a 25 hPa zonal asymmetry and a near-tropopause ozone mixing ratio of 100 ppbv. During JJA the opposite is true; TOMS TTOCs over northern Africa and south Asia likely are underestimated by about 0.5 DU. Accounting for the seasonal variation in tropopause pressure actually slightly increases the discrepancy between TOMS TTOCs and MOZAIC observations.

7. Factors Contributing to the Wave-1 Pattern and the Atlantic Paradox

[51] Distributions of TTOCs from both TOMS and the GEOS-CHEM model (Figure 6) as well as sondes from SHADOZ [Thompson et al., 2002] exhibit a persistent wave-1 amplitude of 13–17 DU with a zonal maximum in TTOCs over the Atlantic and a minimum over the Pacific throughout the year. Here we define the wave-1 amplitude as the peak-to-peak amplitude of a sine wave fitted to the

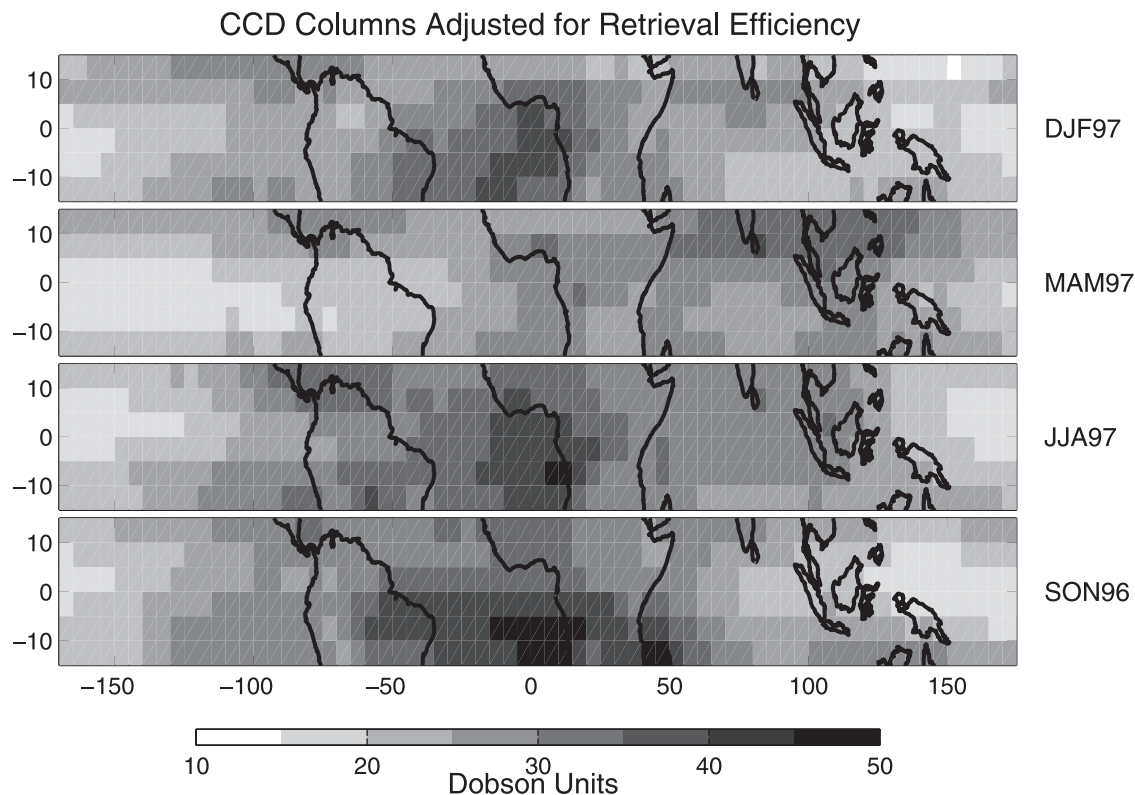## CCD Columns Adjusted for Retrieval Efficiency

Figure 13. Seasonally averaged tropical tropospheric ozone columns (TTOCs) from TOMS for September 1996–August 1997 [*Ziemke et al.*, 1998] in which the efficiency correction described by *Ziemke et al.* [2001] has been replaced by the efficiency correction presented in Figure 12. See color version of this figure at back of this issue.

zonal asymmetry following *Hudson and Thompson* [1998]. Distributions of TTOCs from TOMS and ozonesondes from two ship transects of the tropical Atlantic during January and February also indicate an apparent paradox of more free tropospheric ozone south of the ITCZ (Intertropical Convergence Zone) than north of it [*Weller et al.*, 1996; *Thompson et al.*, 2000]. In this section we show that the persistent wave-1 pattern in TTOCs and the latitudinal gradient over the tropical Atlantic can be explained by (1) the combination of upper tropospheric ozone production largely from lightning NO_x, (2) persistent subsidence over the southern tropical Atlantic as part of the Walker circulation, and (3) cross-equatorial transport of upper tropospheric ozone from northern midlatitudes in the African "westerly duct."

[52] Figure 14 shows the sensitivity of our TTOC simulation to lightning NO_x emissions as determined from a simulation without these emissions. Most of the effect is over the subsiding regions of the eastern Pacific and especially the southern tropical Atlantic despite the concentration of lightning emissions over the continents and in particular over Oceania (Figure 3). Upper level convergence and net subsidence as part of the Walker circulation is strongest over the southern tropical Atlantic throughout the year [*Kalnay et al.*, 1996]. The subsiding air reflects the integrated effect on ozone of lightning emissions in the upwelling branches of the circulation over the tropical continents [*Jacob et al.*, 1996]. We find that lightning enhances TTOCs by 10–15 DU over the tropical Atlantic

and 2–6 DU over the tropical Pacific, explaining almost 60% of the wave-1 amplitude in TTOCs. The remaining fraction is likely explained by the contribution of other NO_x sources to middle and upper tropospheric ozone coupled with the dynamical circulation described above, and by the negative tendency on the ozone column from deep convection over the tropical Pacific [*Lelieveld and Crutzen*, 1994].

[53] Lightning and dynamics also have important roles in the Atlantic paradox as proposed by *Thompson et al.* [2000]. Lightning contributes to the north-south gradient in TTOCs over the tropical Atlantic (Figure 14), with the largest effect during DJF when lightning activity maximizes in the Southern Hemisphere (Figure 3) and particularly persistent subsidence exists over the region [*Kalnay et al.*, 1996]. Figure 14 shows that lightning enhances TTOCs over the southern tropical Atlantic during DJF by 6 DU with respect to the northern tropical Atlantic, making an important contribution to the Atlantic paradox. Lightning NO_x has the smallest effect on TTOCs during JJA when most lightning activity is in the northern tropics, and even then the maximum effect is over the South Atlantic. We find that the sensitivity of TTOCs to lightning in the northern tropics is less than in the southern tropics because of higher background sources of NO_x in the northern hemisphere and hence a lower ozone production efficiency per unit NO_x [*Liu et al.*, 1987].

[54] It is interesting that the lightning enhancement over the southern tropical Atlantic during DJF does not have a

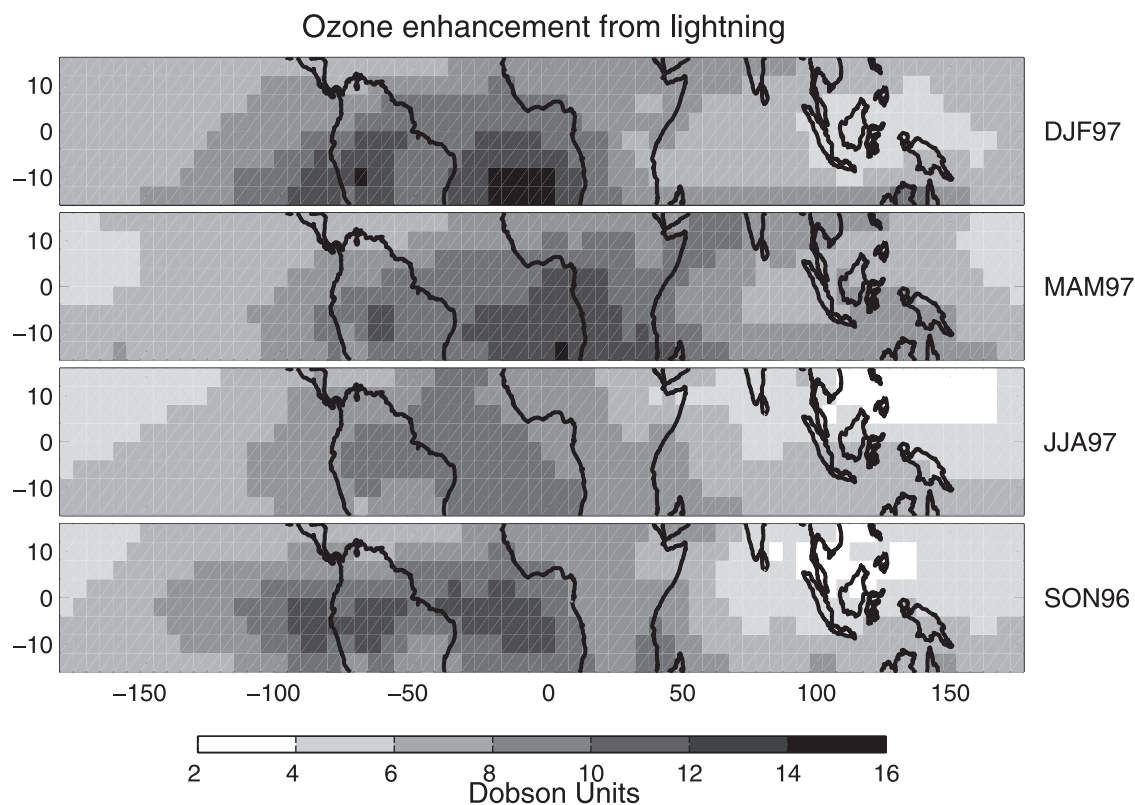## Ozone enhancement from lightning

Figure 14. Ozone column enhancement in the GEOS-CHEM model from lightning emissions, as determined by difference from a simulation without lightning emissions. See color version of this figure at back of this issue.

corresponding signal over the northern tropical Atlantic during JJA (Figure 14). Velocity potential maps [*Kalnay et al.*, 1996] show that upper tropospheric convergence over the southern tropical Atlantic is much stronger than over the northern tropical Atlantic. As illustrated by the ozone flux at 300 hPa (Figure 2a), we find that ozone produced from lightning over northern South America and northern Africa in JJA is transported southward to subside over the southern tropical Atlantic, producing a lightning enhancement there instead of over the northern tropical Atlantic.

[55] We examine the Atlantic paradox of *Thompson et al.* [2000] in more detail using ozonesonde observations from two ship cruises: Aerosols 99 [*Thompson et al.*, 2000] and Polarstern [*Weller et al.*, 1996]. Cruise tracks are shown in Figure 2. Observations show increasing ozone concentrations from the southern to the northern tropical Atlantic at 800 hPa (Figure 15). These ozone concentrations over the northern tropical Atlantic exhibit a biomass burning signature as indicated by their correlation with shipboard measurements of aerosol optical thickness and surface CO [*Thompson et al.*, 2000]. Although the cruises are for different years than the GEOS-CHEM simulation, the model ozone fields at 800 hPa exhibit a similar gradient (Figure 15) driven by outflow from biomass burning over northern Africa (Figure 2).

[56] A gradient reversal occurs in the observations of the upper troposphere with decreasing ozone concentrations from the southern to northern tropical Atlantic at 300 hPa and to a lesser degree at 500 hPa. The GEOS-CHEM simulation does not reproduce the highest values at 300

and 500 hPa and exhibits relatively little north-south gradient. Long-term mean ozone concentrations during January and February over Ascension Island and Natal to the east and west of the cruises show values lower than the cruises but with high variability (Figure 15). Upper tropospheric ozone concentrations measured from aircraft over the southern tropical Atlantic during the TROPOZ II campaign in January 1991 [*Jonquières and Marenco*, 1998] show concentrations of 50–70 ppbv that are more consistent with the climatological observations over Ascension Island than ozonesondes from the two cruises. The southern tropical Atlantic is known to be an important region for intrusions of stratospheric air into the tropics during November through February. Such intrusions could contribute to high variability over the region [*Waugh and Polvani*, 2000]. Indeed, *Weller et al.* [1996] attributed their enhanced upper tropospheric values to a stratospheric influence. The GEOS-CHEM model exhibits almost no stratospheric to tropospheric transport of ozone in the region during December 1996 through February 1997. Anomalous stratospheric intrusions during both cruises, or poor representation of stratospheric to tropospheric exchange in the GEOS fields, may explain the discrepancy between the shipboard observations with both mean values at Ascension and the model. The sensitivity simulation with reduced lightning emissions shows that decreasing the magnitude of lightning NO_x emissions from 6 to 3 Tg N yr^{-1} reduces the latitudinal gradient in the middle and upper troposphere, and results in a model underestimate of even the nonextreme observed ozone concentrations.
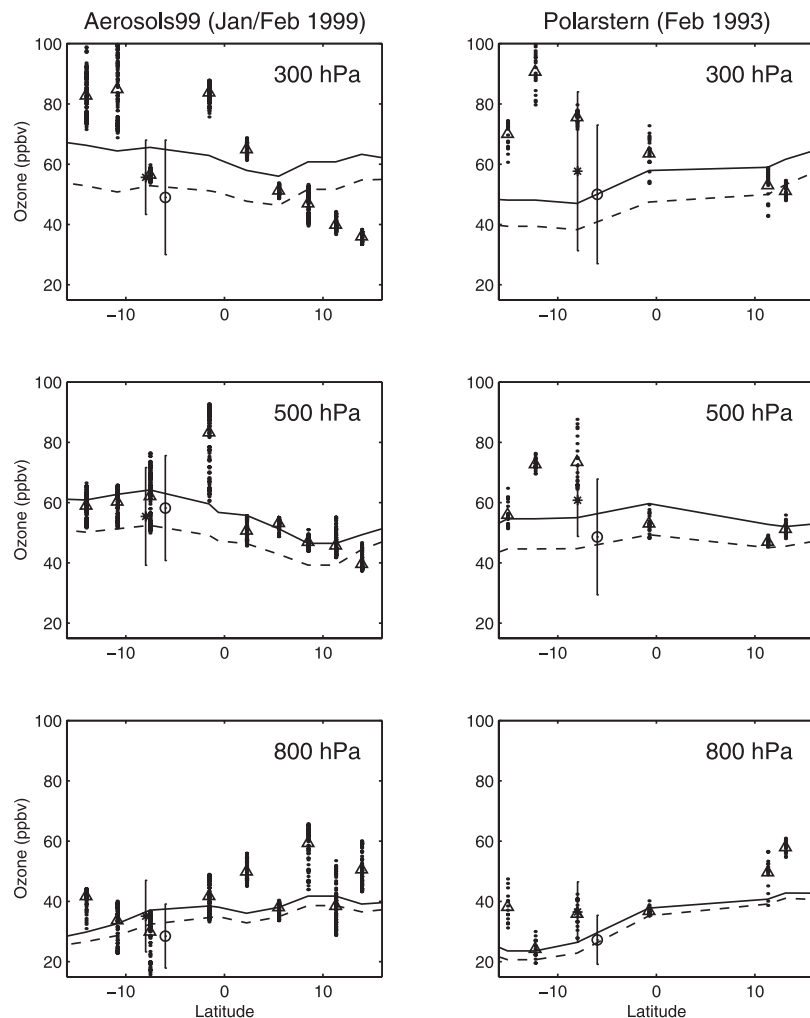
Figure 15. Comparison of ozonesonde observations during the Aerosols99 and Polarstern cruise with the standard GEOS-CHEM simulation (solid), a sensitivity simulation with 3 Tg N yr^{-1} from lightning (dashed). The large black dots represent individual ozonesonde observations within model layers. The black triangles show the mean of the observations within each model layer. The observations are for January 1999 (left) and February 1993 (right) while the model fields are for the corresponding month in 1997. Climatological ozonesonde measurements for the corresponding month are indicated by stars for Ascension Island and open circles for Natal. Error bars indicate one standard deviation.

[57] Figure 2a shows an intrusion of northern hemispheric elevated ozone into the southern tropical Atlantic upper troposphere in January, suggesting that extratropical sources in the northern hemisphere could contribute to the South Atlantic ozone enhancement. *Webster and Holton* [1982] identified the upper troposphere over the tropical Atlantic and eastern Pacific as regions where cross-equatorial propagation of large-scale Rossby waves could occur due to prevailing westerlies, or "westerly ducts" [*Arkin and Webster*, 1985]. *Staudt et al.* [2001] previously demonstrated the importance of the upper tropospheric westerly duct over the eastern Pacific for interhemispheric transport or carbon monoxide; some evidence for this transport is also shown in Figure 2a. To further investigate the possible interhemispheric transport of ozone from northern midlatitudes to the South Atlantic, we examined results from the simulation without lightning emissions, which could provide a confounding factor. In that simulation, we find that upper tropospheric ozone is peeled away from the northern subtropical westerlies toward the southern tropical Atlantic, enhancing ozone concentrations there by 10–15 ppbv relative to the zonal mean. The corresponding tropospheric column enhancement is ~3 DU, explaining 10–20% of the wave-1 amplitude in DJF.

[58] Data from Nimbus 7 TOMS and the temperature humidity infrared radiometer (THIR) sensor have been reanalyzed recently by *Newchurch et al.* [2001b] to suggest that a persistent wave-1 amplitude of about 8 DU (peak-to-peak) exists in stratospheric ozone columns, with a maximum over the tropical Atlantic and a minimum over the tropical Pacific. If such a wave exists, then TTOCs derived using the assumption of a zonally invariant stratospheric column (such as the CCD and MR methods) would overestimate the wave-1 in TTOCs by 8 DU. We find that CCD and MR TTOCs exhibit a peak-to-peak wave-1 of 16 DU and 17 DU respectively when fitted to a sine wave. The magnitude of the feature in both methods is only slightly

Table A1. Aerosol Optical Properties of Dust Particles at 0.4 μm Wavelength[a]

Size Range, μm	r, μm	$\varpi(0)$	Q	ϖ^0	ϖ^1	ϖ^2	ϖ^3	ϖ^4	ϖ^5	ϖ^6	ϖ^7
0.1−0.18	0.15	0.94	2.48	1.0	2.0	2.2	1.7	1.3	0.8	0.5	0.3
0.18−0.3	0.25	0.91	3.10	1.0	2.0	2.5	2.3	2.1	1.7	1.4	1.0
0.3−0.6	0.4	0.86	2.82	1.0	2.0	2.7	2.7	2.9	2.7	2.7	2.5
0.6−1	0.8	0.76	2.43	1.0	2.3	3.3	3.8	4.6	4.9	5.5	5.7
1−1.8	1.5	0.68	2.27	1.0	2.5	3.8	4.8	5.9	6.7	7.7	8.5
1.8−3	2.5	0.62	2.19	1.0	2.7	4.2	5.5	6.8	8.1	9.3	10.5
3−6	4.0	0.58	2.14	1.0	2.8	4.4	5.9	7.5	9.0	10.5	11.9

[a]The dust size classes are from the simulation of *Ginoux et al.* [2001] used as input to the GEOS-CHEM model. For each size class, r is the effective radius, $\varpi(0)$ is the single-scattering albedo, Q is the extinction efficiency, and $\varpi^0-\varpi^7$ are the first eight terms of the Legendre expansion of the scattering phase function.

higher than the 13–14 DU magnitude estimated from SHADOZ data [*Thompson et al.*, 2002] and the 14 DU magnitude in the GEOS-CHEM TTOCs. These results support previous conclusions of an insignificant stratospheric wave-1 as shown by stratospheric data from MLS [*Ziemke et al.*, 1996], MLS and HALOE [*Ziemke et al.*, 1998], and ozonesondes [*Thompson et al.*, 2002].

8. Conclusions

[59] We used a global 3-D model of tropospheric chemistry (GEOS-CHEM) to simulate the tropical tropospheric ozone columns (TTOCs) retrieved from the Total Ozone Mapping Spectrometer (TOMS), and explored the discrepancies through further analyses of in situ observations and of the TOMS retrieval algorithm. The version of the GEOS-CHEM model used here was improved in several ways over that reported by *Bey et al.* [2001a], in particular with a revised biomass burning inventory and inclusion of the photochemical effects of mineral dust. A global lightning NO_x source of 6 Tg N yr^{-1} in the model produced a simulation that is most consistent with TOMS and in situ observations. The simulation explains 56% of the observed variance in TTOCs (10°S–10°N) derived from the convective cloud differential (CCD) method [*Ziemke et al.*, 1998] and 41% of that derived from the modified residual (MR) method. There is no global bias in the simulation of either TOMS TTOC product. Radiative and heterogeneous chemical effects of mineral dust have only a minor role in the modeled distribution of TTOCs due to competing influences; effects are larger on other trace gases including a 9% decrease of the global mean OH concentration weighted by reaction with methane (Appendix A).

[60] Over sub-Saharan northern Africa and south Asia, the TOMS TTOCs do not capture the seasonal maximum from biomass burning found in the MOZAIC aircraft observations and in the model. A characteristic feature of this seasonal maximum, in contrast to the southern tropics, is that it is driven by the lower troposphere where the sensitivity of TOMS is relatively poor due to Rayleigh scattering. We used a radiative transfer model (LIDORT), local surface albedos from TOMS, and the GEOS-CHEM model to derive an efficiency correction to the TOMS retrieval algorithm to account for the insensitivity of TOMS to ozone in the lower troposphere. We calculated the efficiency correction as the difference between the standard ozone profiles in the TOMS retrieval algorithm and the monthly mean GEOS-CHEM fields, weighted by the

TOMS sensitivity. The efficiency correction increased TTOCs over biomass burning regions by 3–5 Dobson units (DU) and decreased them by 2–5 DU over oceanic regions, explaining 13% of the variance between CCD and GEOS-CHEM TTOCs and improving the agreement between CCD TTOCs and in situ observations. The correction is available from the authors. The correction reduces the magnitude of the "tropical Atlantic paradox" [*Thompson et al.*, 2000], i.e., the north-south gradient reversal in ozone over the tropical Atlantic during the northern African biomass burning season in December–February (DJF) as observed by TTOCs and ozonesondes from ship cruises. The CCD TTOCs over the southern tropical Atlantic are reduced by 10 DU relative to northern Africa during DJF. Even after this correction, a TTOC enhancement during DJF is still present over the southern tropical Atlantic. We reproduce this enhancement in the model and explain it by the combination of upper tropospheric ozone production from lightning NO_x, persistent subsidence over the southern tropical Atlantic as part of the Walker circulation, and cross-equatorial transport of upper tropospheric ozone from northern midlatitudes in the African "westerly duct."

[61] Distributions of TTOCs from TOMS, the GEOS-CHEM model, and sondes exhibit a persistent wave-1 amplitude of 13–17 DU with a zonal maximum in TTOCs over the Atlantic and a minimum over the Pacific throughout the year. Upper tropospheric ozone production from lightning NO_x, combined with the large-scale Walker circulation, largely explains the wave-1 pattern in the model. We find that the influence of lightning on TTOCs is strongest over subsiding regions such as the tropical Atlantic and weakest over upwelling regions such as the tropical Pacific. It seems unlikely that a significant wave-1 exists in tropical stratospheric ozone columns.

[62] The TOMS overestimate of tropospheric ozone over northern Africa during June through October represents a significant problem that is not completely explained by our efficiency correction. The broader spectral range offered by instruments such as the Global Ozone Monitoring Experiment (GOME) [*Burrows et al.*, 1999] should be useful to determine what is interfering with the TOMS measurement of ozone over this region.

[63] The next generation of space-based instruments also holds promise for understanding the model overestimates of ozone over the South Pacific and south Asia. Uncertainty in the global distribution of lightning may be significant over the Pacific, while uncertainties in heterogeneous chemistry and emissions from India may be important issues over south Asia. Direct sensing of tropo-

Table A2. Complex Refractive Indices Used to Calculate Mineral Dust Radiative Properties[a]

Wavelength, μm	Refractive Index
0.3	$1.60 - 0.024i$
0.4	$1.58 - 0.014i$
0.6	$1.55 - 0.004i$
1.0	$1.54 - 0.005i$

[a] Data are from *Patterson et al.* [1977].

spheric ozone, as with the Tropospheric Emission Spectrometer (TES) [*Clough et al.*, 1995; *Beer et al.*, 2001; *Luo et al.*, 2002], as well as ozone precursors from GOME, TES, and other instruments should provide considerable insight into these problems.

Appendix A: Photochemical Effects of Mineral Dust

A1. Implementation in GEOS-CHEM

[64] The radiative and heterogeneous chemical effects of dust are potentially an important consideration for the simulation of tropospheric ozone, particularly over northern Africa and eastern Asia [*Zhang et al.*, 1994; *Dentener et al.*, 1996; *Zhang and Carmichael*, 1999; *De Reus et al.*, 2000; *Phadnis and Carmichael*, 2000]. Recently, the TOMS aerosol index [*Herman et al.*, 1997; *Torres et al.*, 1998] has been used to identify sources of mineral dust [*Prospero et al.*, 2002] and to improve the global simulation of dust distributions [*Ginoux et al.*, 2001]. In the present simulation we use global 3-D monthly mean model fields of size-

resolved mineral dust from *Ginoux et al.* [2001] determined with GEOS meteorological fields for the 1996−97 simulation period (Table A1). *Ginoux et al.* [2001] showed that their dust fields are generally consistent with observed dust concentrations, surface deposition, and optical thickness throughout the tropics, but concentrations and surface deposition over the tropical Pacific are biased high by a factor of 2−5, and the simulated size distribution generally underestimates large particles and overestimates small particles by about a factor of 2.

[65] To account for the radiative effects of mineral dust in GEOS-CHEM, we calculate the single scattering albedo, the extinction efficiency, and the first eight terms in the Legendre expansion of the phase function, for each of the seven particle sizes in Table A1 and the four wavelengths in Table A2, using a Mie algorithm [*de Rooij and van der Stap*, 1984; *Mishchenko et al.*, 1999]. In the Mie calculation, we assume a standard gamma size distribution with effective variance of 0.2 for each of the seven particle sizes. The complex refractive indices (Table A2) are from bulk samples of far-traveled Saharan dust [*Patterson et al.*, 1977] as provided by A. Lacis (personal communication, 2000). The resulting dust optical properties are added as a dust aerosol to the Fast-J radiative transfer code of *Wild et al.* [2000]. Table A1 gives the optical properties at 0.4 μm. Single scattering albedos range from 0.58 to 0.94, decreasing with increasing particle size. Single scattering albedos at 0.3 μm are about 85% of the values at 0.4 μm.

[66] We calculate the dust optical depth τ from the mass concentration, extinction efficiency, and particle mass density for each particle size and wavelength. Figure A1
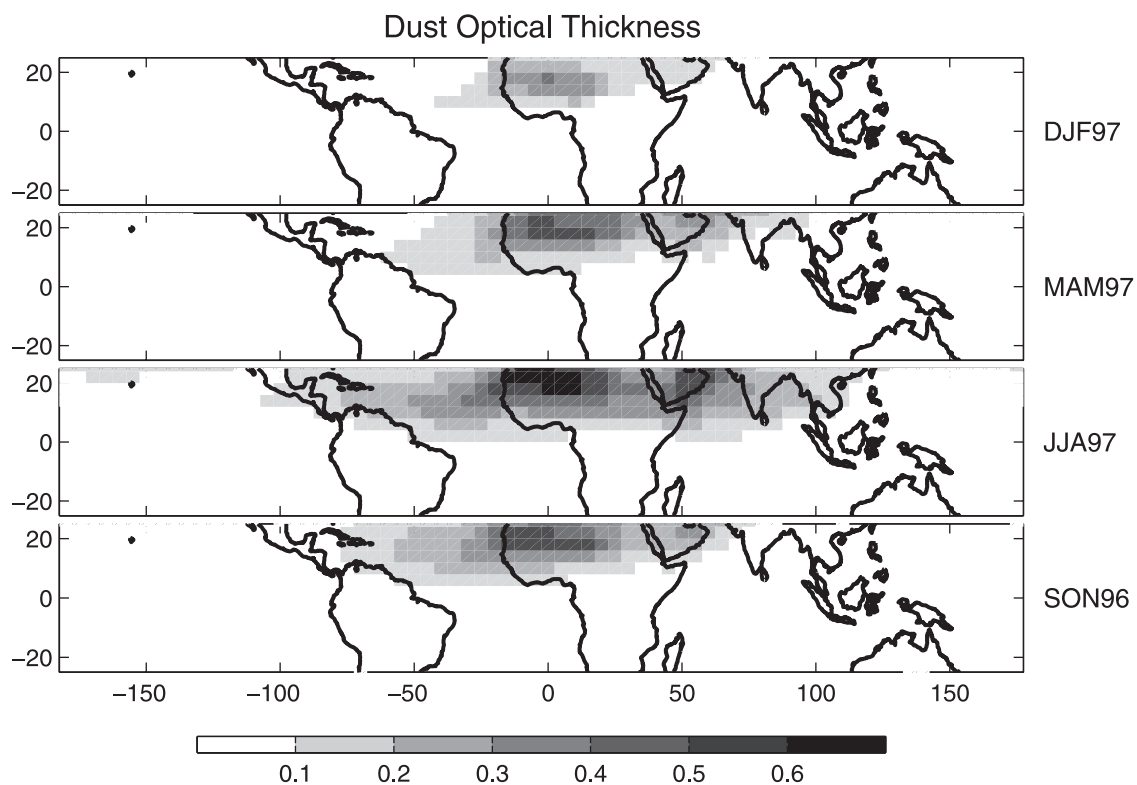

Figure A1. Seasonally averaged dust optical thickness at 0.4 μm for September 1996−August 1997 calculated from mass concentrations provided by *Ginoux et al.* [2001].
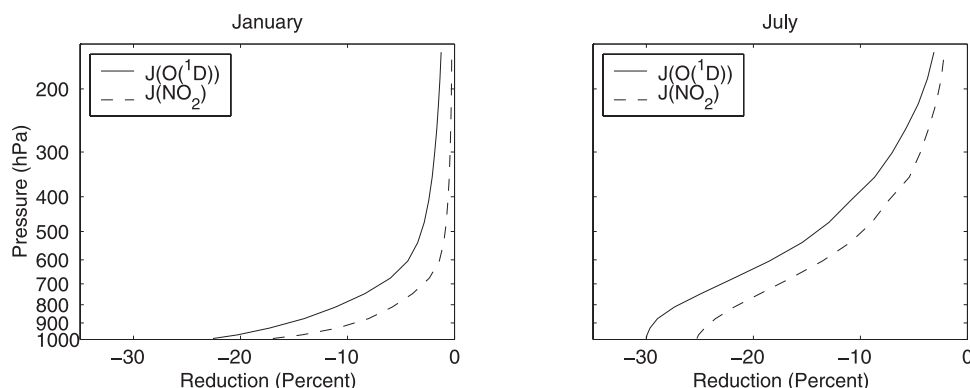
Figure A2.   Reduction in photolysis frequencies for an illustrative column over northern Africa (10°N, 15°E) due to scattering and absorption by mineral dust.

illustrates the spatial and seasonal variation of τ at 0.4 μm summed over all seven particle sizes. Particles between 0.6–1.8 μm account for most of τ. The tropical dust column is minimum during DJF and maximum during JJA and is strongly centered over northern Africa.

[67]   We find that dust causes the actinic flux to decrease at all altitudes. Figure A2 shows the effect for an illustrative region over northern Africa. There is little dust above 700 hPa in January. The dust layer is more vertically mixed

during July when convective activity is more intense. At the surface, monthly mean J(NO$_2$) decreases by up to 15% in January and 25% in July while J[O(^{1}D)] decreases by up to 20% in January and 30% in July.

[68]   We implement heterogeneous chemistry on the mineral dust aerosol surfaces in GEOS-CHEM following the reaction probability formulation already in place for sulfate aerosols [*Bey et al.*, 2001a]. The rate constant k for chemical loss of a gas with mean molecular speed v and gas-phase
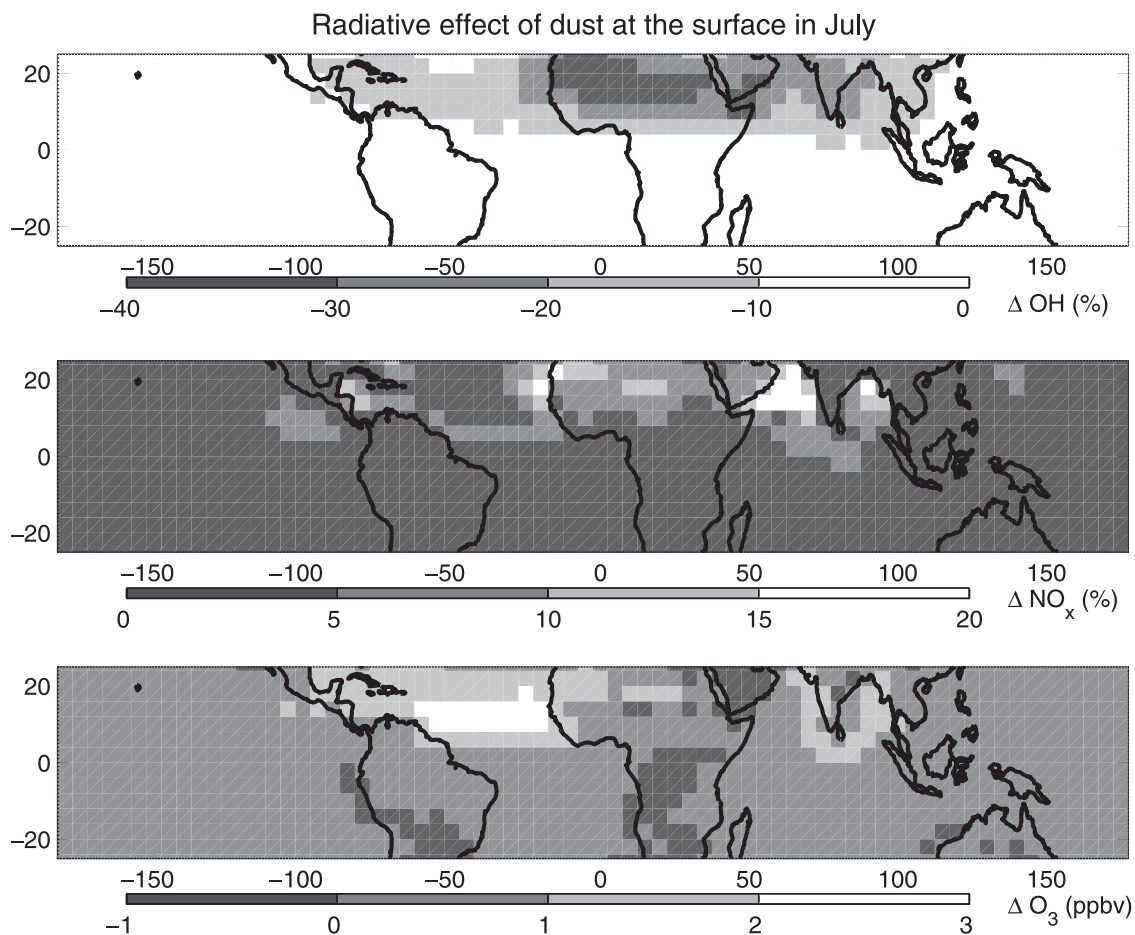
Figure A3.   Mean changes in OH, NO$_x$, and ozone due to the radiative effects of mineral dust at the surface in July, as determined by the difference with a simulation without dust.
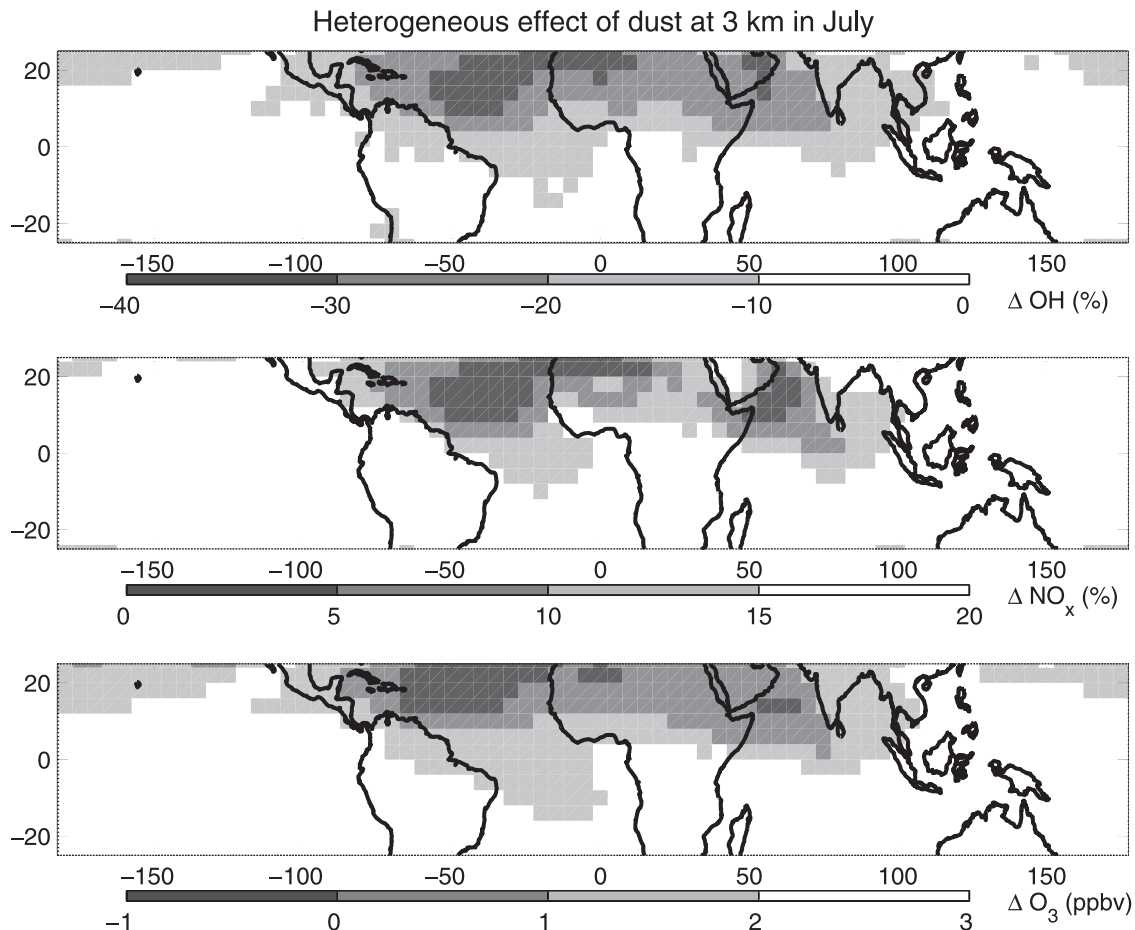
Heterogeneous effect of dust at 3 km in July

Figure A4. Mean changes in OH, NO_x, and ozone due to the heterogeneous chemical effects of mineral dust at 3 km in July, as determined by the difference with a simulation without the heterogeneous chemical effects of dust.

molecular diffusion coefficient D_g on an aerosol of particle radius a is given by

$$k = \left(\frac{a}{D_g} + \frac{4}{v\gamma} \right)^{-1} A, \qquad (A1)$$

where γ is the reaction probability that a molecule impacting the aerosol surface undergoes reaction [*Ravishankara*, 1997], and A is the aerosol surface area per unit volume of air. We include the four heterogeneous reactions $HO_2 \rightarrow 0.5\,H_2O_2$, $NO_2 \rightarrow 0.5\,HONO + 0.5\,HNO_3$, $NO_3 \rightarrow HNO_3$, and $N_2O_5 \rightarrow 2\,HNO_3$ with reaction probabilities of 0.2, 10^{-4}, 10^{-3}, and 0.1, respectively, as recommended by *Jacob* [2000]. For the range of particle sizes and γ values used here, the chemical rate constant k may be limited either by free molecular collision ($4/v\gamma$ term in equation A1) or by diffusion (a/D_g term).

[69] No measurements exist for ozone uptake by dust. Direct uptake of ozone by dust has been postulated by *Dentener et al.* [1996] with an assumed γ of $10^{-4}–10^{-5}$ based on analogy with measured ozone deposition to bare soil, however ozone deposition to soil most likely involves reaction with unsaturated organics, and the analogy to suspended dust may not hold. In addition, laboratory measurements [*Moise and Rudich*, 2000] show that ozone uptake by organic aerosol surfaces is rapidly quenched as

surface reaction sites are oxidized. It appears that fast reaction between ozone and organic compounds on dust surfaces would titrate the organic compounds without affecting ozone significantly.

A2. Effects of Mineral Dust

[70] We find two competing radiative effects from dust on ozone in the GEOS-CHEM simulation. The direct effect decreases OH and ozone production due to the reduced actinic flux. As a result of the reduced OH, the CH_3CCl_3 lifetime increases by 0.3 years (Table 2). The indirect effect increases ozone production outside of dust regions by increasing the lifetime of ozone precursors. Figure A3 illustrates the combined effect at the surface. Over northern Africa, maximum decreases in OH are 10–20% during January and 20–40% during July. Over the same region NO_x increases by up to 4% during January and 20% during July. Ozone remains largely unchanged, decreasing by a few ppbv near the surface of northern Africa during January and increasing by up to 3 ppbv over the Atlantic in July. Overall we find that the combined direct and indirect effects lead to negligible net changes of -0.4 to 0.8 DU in TTOCs. The concentrations of other trace gases increase throughout the troposphere by up to 50% for PAN, 10% for CO, as well as 15% for upper tropospheric acetone, peroxides, and aldehydes.

[71] Heterogeneous chemistry on mineral dust decreases ozone throughout the troposphere due to the loss of both HO_x and NO_x radicals. The heterogeneous reactions increase the CH_3CCl_3 lifetime by 0.2 years (Table 2). Figure A4 illustrates the effect of chemical reactions on mineral dust at 3 km in July. Throughout the lower 5 km OH, NO_x, and ozone decrease by up to 15%, 30%, and 10%, respectively. As dust concentrations decrease above these altitudes, so does their effect upon trace gases. Ozone decreases in the upper troposphere during January and July by about 1% and 2%, respectively. Over northern Africa and the northern tropical Atlantic TTOCs decrease by 1–2 DU, and decrease less than 1 DU elsewhere. The largest decrease occurs over the northern tropical Atlantic where radiative effects cause the largest increase, resulting in compensation of effects (Figure 7).

[72] The combined radiative and chemical effects of mineral dust globally decrease OH by 9% (weighted by the amount of CH_3CCl_3 or methane reacting with OH).

References

Allen, D., and K. Pickering, Evaluation of lightning flash rate parameterizations for use in a global chemical transport model, *J. Geophys. Res.*, *107*, doi:10.1029/2002JD002066, in press, 2002.

Allen, D. J., K. E. Pickering, and A. Molod, An evaluation of deep convective mixing in the Goddard Chemical Transport Model using International Satellite Cloud Climatology Project cloud parameters, *J. Geophys. Res.*, *102*, 25,467–25,476, 1997.

Andreae, M. O., A. Chapuis, B. Cros, J. Fontan, G. Helas, C. Justice, Y. J. Kaufman, A. Minga, and D. Nganga, Ozone and Aitken nuclei over equatorial Africa: Airborne observations during DECAFE 88, *J. Geophys. Res.*, *97*, 6137–6148, 1992.

Arino, O., and J.-M. Rosaz, 1997 and 1998 World ATSR Fire Atlas using ERS-2 ATSR-2 data, paper presented at the Joint Fire Science Conference, Univ. of Idaho and Int. Assoc. of Wildland Fire, Boise, Idaho, 1999.

Arkin, P. A., and P. J. Webster, Annual and interannual variability of tropical-extratropical interaction: An empirical study, *Mon. Weather Rev.*, *113*, 1510–1523, 1985.

Beer, R., T. A. Glavich, and D. M. Rider, Tropospheric emission spectrometer for the Earth Observing System's Aura satellite, *Appl. Opt.*, *40*, 2356–2367, 2001.

Bell, N., L. Hsu, D. J. Jacob, M. G. Schultz, D. R. Blake, J. Butler, D. B. King, J. M. Lobert, and E. Maier-Remier, Methyl iodide: Atmospheric budget and use as a tracer of marine convection in global models, *J. Geophys. Res.*, *107*, doi:10.1029/2001JD001151, in press, 2002.

Benkovitz, C. M., M. T. Schultz, J. Pacyna, L. Tarrason, J. Dignon, E. C. Voldner, P. A. Spiro, J. A. Logan, and T. E. Graedel, Global gridded inventories of anthropogenic emissions of sulfur and nitrogen, *J. Geophys. Res.*, *101*, 29,239–29,253, 1996.

Bey, I., D. J. Jacob, R. M. Yantosca, J. A. Logan, B. D. Field, A. M. Fiore, Q. Li, H. Y. Liu, L. J. Mickley, and M. G. Schultz, Global modeling of tropospheric chemistry with assimilated meteorology: Model description and evaluation, *J. Geophys. Res.*, *106*, 23,073–23,096, 2001a.

Bey, I., D. J. Jacob, J. A. Logan, and R. M. Yantosca, Asian chemical outflow to the Pacific in spring: Origins, pathways and budgets, *J. Geophys. Res.*, *106*, 23,097–23,114, 2001b.

Burrows, J. P., et al., The Global Ozone Monitoring Experiment (GOME): Mission concept and first scientific results, *J. Atmos. Sci.*, *56*, 151–175, 1999.

Chandra, S., J. R. Ziemke, W. Min, and W. G. Read, Effects of 1997–1998 El Niño on tropospheric ozone and water vapor, *Geophys. Res. Lett.*, *25*, 3867–3870, 1998.

Chandra, S., J. R. Ziemke, P. K. Bhartia, and R. V. Martin, Tropical tropospheric ozone: Implications for dynamics and biomass burning, *J. Geophys. Res.*, *107*(D14), 4188, doi:10.1029/2001JD000447, 2002.

Chin, M., P. Ginoux, S. Kinne, O. Torres, B. Holben, B. N. Duncan, R. V. Martin, J. A. Logan, A. Higurashi, and T. Nakajima, Tropospheric aerosol optical thickness from the GOCART model and comparisons with satellite and sunphotometer measurements, *J. Atmos. Sci.*, *59*, 461–483, 2002.

Clough, S. A., C. P. Rinsland, and P. D. Brown, Retrieval of tropospheric ozone from simulations of nadir spectral radiances as observed from space, *J. Geophys. Res.*, *100*, 16,579–16,593, 1995.

Craig, R. A., *The Upper Atmosphere: Metorology and Physics*, Academic, San Diego, Calif., 1965.

Crawford, J., et al., Photostationary state analysis of the NO_2-NO system based on airborne observations from the western and central North Pacific, *J. Geophys. Res.*, *101*, 2053–2072, 1996.

De Reus, M., F. Dentener, A. Thomas, S. Borrmann, J. Ström, and J. Lelieveld, Airborne observations of dust aerosol over the North Atlantic Ocean during ACE 2: Indications for heterogeneous ozone destruction, *J. Geophys. Res.*, *105*, 15,263–15,275, 2000.

de Rooij, W. A., and C. C. A. H. van der Stap, Expansion of Mie scattering matrices in generalized spherical functions, *Astron. Astrophys.*, *131*, 237–248, 1984.

Dentener, F. J., G. R. Carmichael, Y. Zhang, J. Lelieveld, and P. J. Crutzen, Role of mineral aerosol as a reactive surface in the global troposphere, *J. Geophys. Res.*, *101*, 22,869–22,889, 1996.

Fiore, A. M., D. J. Jacob, I. Bey, R. M. Yantosca, B. D. Field, and J. G. Wilkinson, Background ozone over the United States in summer: Origin, trend, and contribution to pollution episodes, *J. Geophys. Res.*, *107*(D15), 4275, doi:10.1029/2001JD000982, 2002.

Fishman, J., and A. E. Balok, Calculation of daily tropospheric ozone residuals using TOMS and empirically improved SBUV measurements: Application to an ozone pollution episode over the eastern United States, *J. Geophys. Res.*, *104*, 30,319–30,340, 1999.

Fishman, J., C. E. Watson, J. C. Larsen, and J. A. Logan, Distribution of tropospheric ozone determined from satellite data, *J. Geophys. Res.*, *95*, 3599–3617, 1990.

Fishman, J., J. M. Hoell, R. D. Bendura, R. J. McNeil, and V. W. J. H. Kirchhoff, NASA GTE TRACE A experiment (September–October 1992): Overview, *J. Geophys. Res.*, *101*, 23,865–23,879, 1996.

Folkins, I., M. Loewenstein, J. Podolske, S. J. Oltmans, and M. Proffitt, A barrier to vertical mixing at 14 km in the tropics: Evidence from ozonesondes and aircraft measurements, *J. Geophys. Res.*, *104*, 22,095–22,102, 1999.

Fontan, J., A. Druilhet, B. Benech, R. Lyra, and B. Cros, The DECAFE experiments: Overview and meteorology, *J. Geophys. Res.*, *97*, 6123–6136, 1992.

Galanter, M., H. Levy II, and G. R. Carmichael, Impacts of biomass burning on tropospheric CO, NO_x, and O_3, *J. Geophys. Res.*, *105*, 6633–6653, 2000.

Ginoux, P., M. Chin, I. Tegen, J. M. Prospero, B. Holben, O. Dubovik, and S. Lin, Sources and distributions of dust aerosols simulated with the GOCART model, *J. Geophys. Res.*, *106*, 20,255–20,274, 2001.

Guenther, A., et al., A global model of natural volatile organic compound emissions, *J. Geophys. Res.*, *100*, 8873–8892, 1995.

Hauglustaine, D. A., G. P. Brasseur, S. Walters, P. J. Rasch, J.-F. Müller, L. K. Emmons, and M. A. Carroll, MOZART, a global chemical transport model for ozone and related chemical tracers, 2, Model results and evaluation, *J. Geophys. Res.*, *103*, 28,291–28,335, 1998.

Herman, J. R., and E. A. Celarier, Earth surface reflectivity climatology at 340–380 nm from TOMS data, *J. Geophys. Res.*, *102*, 28,003–28,011, 1997.

Herman, J. R., P. K. Bhartia, O. Torres, C. Hsu, C. Seftor, and E. Celarier, Global distributions of UV-absorbing aerosols from Nimbus 7/TOMS data, *J. Geophys. Res.*, *102*, 16,911–16,922, 1997.

Highwood, E. J., and B. J. Hoskins, The tropical tropopause, *Q. J. R. Meteorol. Soc.*, *124*, 1579–1604, 1998.

Hoell, J. M., D. D. Davis, D. J. Jacob, M. O. Rogers, R. E. Newell, H. E. Fuelberg, R. J. McNeal, J. L. Raper, and R. J. Bendura, Pacific Exploratory Mission in the Pacific: PEM Tropics A, August–September 1996, *J. Geophys. Res.*, *104*, 5567–5584, 1999.

Houghton, J. T., Y. Ding, D. J. Griggs, M. Noguer, P. J. van der Linden, X. Dai, K. Maskell, and C. A. Johnson, *Climate Change 2001*, Cambridge Univ. Press, New York, 2001.

Hudson, R. D., and A. M. Thompson, Tropical tropospheric ozone from total ozone mapping spectrometer by a modified residual method, *J. Geophys. Res.*, *103*, 22,129–22,145, 1998.

Hudson, R. D., J.-H. Kim, and A. M. Thompson, On the derivation of tropospheric column ozone from radiances measured by the total ozone mapping spectrometer, *J. Geophys. Res.*, *100*, 11,137–11,145, 1995.

Jacob, D. J., Heterogeneous chemistry and tropospheric ozone, *Atmos. Environ.*, *34*, 2131–2159, 2000.

Jacob, D. J., et al., Origin of ozone and NO_x in the tropical troposphere: A photochemical analysis of aircraft observations over the South Atlantic basin, *J. Geophys. Res.*, *101*, 24,235–24,250, 1996.

Jacob, D. J., B. D. Field, E. Jin, I. Bey, Q. Li, J. A. Logan, and R. M. Yantosca, Atmospheric budget of acetone, *J. Geophys. Res.*, *107*(D10), 4100, doi:10.1029/2001JD000694, 2002.

Jacobson, M. Z., and R. P. Turco, SMVGEAR: A sparse-matrix, vectorized Gear code for atmospheric models, *Atmos. Environ.*, *28*, 273–284, 1994.

Jonquières, I., and A. Marenco, Redistribution by deep convection and long-range transport of CO and CH_4 emissions from the Amazon basin, as observed by the airborne campaign TROPOZ II during the wet season, *J. Geophys. Res.*, *103*, 19,075–19,091, 1998.

Jourdain, L., and D. A. Hauglustaine, The global distribution of lightning NO_x simulated on-line in a general circulation model, *Phys. Chem. Earth, Part C*, *26*, 585–591, 2001.

Kalnay, E., et al., The NCEP/NCAR 40-year reanalysis project, *Bull. Am. Meteorol. Soc.*, *77*, 437–471, 1996.

Kim, J. H., M. J. Newchurch, and K. Han, Distribution of tropical tropospheric ozone determined by the scan-angle method applied to TOMS measurements, *J. Atmos. Sci.*, *58*, 2699–2708, 2001.

Klenk, K. F., P. K. Bhartia, A. J. Fleig, V. G. Kaveeshwar, R. D. McPeters, and P. M. Smith, Total ozone determination from the backscattered ultraviolet (BUV) experiment, *J. Appl. Meteorol.*, *21*, 1672–1684, 1982.

Krishnamurti, T. N., H. Fuelberg, M. C. Sinha, D. Oosterhof, E. L. Bensman, and V. B. Kumar, The meteorological environment of the tropospheric ozone maximum over the tropical South Atlantic Ocean, *J. Geophys. Res.*, *98*, 10,621–10,641, 1993.

Krishnamurti, T. N., M. C. Sinha, M. Kanamitsu, D. Oosterhof, H. Fuelberg, R. Chatfield, D. J. Jacob, and J. Logan, Passive tracer transport relevant to the TRACE A experiment, *J. Geophys. Res.*, *101*, 23,889–23,907, 1996.

Lal, S., and M. G. Lawrence, Elevated mixing ratios of surface ozone over the Arabian Sea, *Geophys. Res. Lett.*, *28*, 1487–1490, 2001.

Law, K. S., P.-H. Plantevin, V. Thouret, A. Marenco, W. A. H. Asman, M. Lawrence, P. J. Crutzen, J. F. Müller, D. A. Hauglustaine, and M. Kanakidou, Comparison between global chemistry transport model results and measurement of ozone and water vapor by Airbus in-Service Aircraft (MOZAIC) data, *J. Geophys. Res.*, *105*, 1503–1525, 2000.

Lawrence, M. G., P. J. Crutzen, P. J. Rasch, B. E. Eaton, and N. M. Mahowald, A model for studies of tropospheric photochemistry: Description, global distributions, and evaluation, *J. Geophys. Res.*, *104*, 26,245–26,277, 1999.

Lee, D. S., I. Köhler, E. Grobler, F. Rohrer, R. Sausen, L. Gallardo-Klenner, J. H. I. Olivier, F. J. Dentener, and A. F. Bouwman, Estimations of global NO_X emissions and their uncertainties, *Atmos. Environ.*, *31*, 1735–1749, 1997.

Lelieveld, J., and P. J. Crutzen, Role of deep cloud convection in the ozone budget of the troposphere, *Science*, *264*, 1759–1761, 1994.

Lelieveld, J., and F. J. Dentener, What controls tropospheric ozone?, *J. Geophys. Res.*, *105*, 3531–3551, 2000.

Lelieveld, J., et al., The Indian Ocean Experiment: Widespread air pollution from south and Southeast Asia, *Science*, *291*, 1031–1035, 2001.

Levy, H., W. J. Moxim, and P. S. Kasibhatla, A global three-dimensional time-dependent lightning source of tropospheric NO_x, *J. Geophys. Res.*, *101*, 22,911–22,922, 1996.

Li, Q., D. J. Jacob, I. Bey, R. M. Yantosca, Y. Zhao, Y. Kondo, and J. Notholt, Atmospheric hydrogen cyanide (HCN): Biomass burning source, ocean sink?, *Geophys. Res. Lett.*, *27*, 357–360, 2000.

Li, Q., et al., A tropospheric ozone maximum over the Middle East, *Geophys. Res. Lett.*, *28*, 3235–3238, 2001.

Li, Q., et al., Transatlantic transport of pollution and its effect on surface ozone in Europe and North America, *J. Geophys. Res.*, *107*(D13), doi:10.1029/2001JD001422, 2002a.

Li, Q., D. J. Jacob, T. D. Fairlie, H. Liu, R. M. Yantosca, and R. V. Martin, Stratospheric versus pollution influences on ozone at Bermuda: Reconciling past analyses, *J. Geophys. Res.*, *107*, doi:10.1029/2002JD002138, in press, 2002b.

Liu, H., D. J. Jacob, I. Bey, and R. M. Yantosca, Constraints from ^{210}Pb and ^{7}Be on wet deposition and transport in a global three-dimensional chemical tracer model driven by assimilated meteorological fields, *J. Geophys. Res.*, *106*, 12,109–12,128, 2001.

Liu, H., D. J. Jacob, L. Y. Chan, S. J. Oltmans, I. Bey, R. M. Yantosca, J. M. Harris, B. N. Duncan, and R. V. Martin, Sources of tropospheric ozone along the Asian Pacific Rim: An analysis of ozonesonde observations, *J. Geophys. Res.*, *107*, doi:10.1029/2001JD002005, in press, 2002.

Liu, S. C., M. Trainer, F. C. Fehsenfeld, D. D. Parrish, E. J. Williams, D. W. Fahey, G. Hubler, and P. C. Murphy, Ozone production in the rural troposphere and implications for regional and global ozone distributions, *J. Geophys. Res.*, *92*, 10,463–10,482, 1987.

Lobert, J. M., W. C. Keene, J. A. Logan, and R. Yevich, Global chlorine emissions from biomass burning: Reactive chlorine emissions inventory, *J. Geophys. Res.*, *104*, 8373–8390, 1999.

Logan, J. A., An analysis of ozonesonde data for the troposphere: Recommendations for testing three-dimensional models and development of a gridded climatology for tropospheric ozone, *J. Geophys. Res.*, *104*, 16,115–16,149, 1999.

Luo, M., R. Beer, D. J. Jacob, J. A. Logan, and C. D. Rodgers, Simulated observation of tropospheric ozone and CO with the Tropospheric Emission Spectrometer (TES) satellite instrument, *J. Geophys. Res.*, *107*(D15), 4270, doi:10.1029/2001JD000804, 2002.

Marenco, A., J. C. Medale, and S. Prieur, Study of tropospheric ozone in the tropical belt (Africa, America) from STRATOZ and TROPOZ campaigns, *Atmos. Environ.*, *24A*, 2823–2834, 1990.

Marenco, A., et al., Measurement of ozone and water vapor by Airbus in-service aircraft: The MOZAIC airborne program, an overview, *J. Geophys. Res.*, *103*, 25,631–25,642, 1998.

Martin, R. V., D. J. Jacob, J. A. Logan, J. R. Ziemke, and R. Washington, Detection of a lightning influence on tropical tropospheric ozone, *Geophys. Res. Lett.*, *27*, 1639–1642, 2000.

Martin, R. V., et al., An improved retrieval of tropospheric nitrogen dioxide from GOME, *J. Geophys. Res.*, *107*, doi:10.1029/2001JD001027, in press, 2002.

McLinden, C. A., S. C. Olsen, B. Hannegan, O. Wild, M. J. Prather, and J. Sundet, Stratospheric ozone in 3-D models: A simple chemistry and the cross-tropopause flux, *J. Geophys. Res.*, *105*, 14,653–14,665, 2000.

McPeters, R. D., et al., Earth Probe Total Ozone Mapping Spectrometer (TOMS) data, in *Data Products User's Guide*, *NASA Tech. Publ.*, *1998-206895*, 1998.

Mickley, L. J., P. P. Murti, D. J. Jacob, J. A. Logan, D. Koch, and D. Rind, Radiative forcing from tropospheric ozone calculated with a unified chemistry-climate model, *J. Geophys. Res.*, *104*, 30,153–30,172, 1999.

Mishchenko, M. I., J. M. Dlugach, E. G. Yanovitskij, and N. T. Zakharova, Bidirectional reflectance of flat optically thick particulate layers: An efficient radiative transfer solution and applications to snow and soil surfaces, *J. Quant. Spectrosc. Radiat. Transfer*, *63*, 409–432, 1999.

Moise, T., and Y. Rudich, Reactive uptake of ozone by proxies for organic aerosols: Surface versus bulk processes, *J. Geophys. Res.*, *105*, 14,667–14,676, 2000.

Moxim, W. J., and H. Levy, A model analysis of the tropical South Atlantic Ocean tropospheric ozone maximum: The interaction of transport and chemistry, *J. Geophys. Res.*, *105*, 17,393–17,415, 2000.

Newchurch, M. J., X. Liu, and J. H. Kim, Lower-tropospheric ozone (LTO) derived from TOMS near mountainous regions, *J. Geophys. Res.*, *106*, 20,403–20,412, 2001a.

Newchurch, M. J., D. Sun, and J. H. Kim, Zonal wave-1 structure in TOMS tropical stratospheric ozone, *Geophys. Res. Lett.*, *28*, 3151–3154, 2001b.

Oltmans, S. J., et al., Trends of ozone in the troposphere, *Geophys. Res. Lett.*, *25*, 139–142, 1998.

Oltmans, S. J., et al., Ozone in the Pacific tropical troposphere from ozonesonde observations, *J. Geophys. Res.*, *106*(D23), 10.1029/2000900834, 2002.

Palmer, P. I., D. J. Jacob, K. Chance, R. V. Martin, R. J. D. Spurr, T. P. Kurosu, I. Bey, R. Yantosca, A. Fiore, and Q. Li, Air mass factor formulation for spectroscopic measurements from satellites: Application to formaldehyde retrievals from the Global Ozone Monitoring Experiment, *J. Geophys. Res.*, *106*, 14,539–14,550, 2001.

Palmer, P. I., D. J. Jacob, A. M. Fiore, R. V. Martin, K. Chance, and T. P. Kurosu, Mapping isoprene emissions over North America using formaldehyde column observations from space, *J. Geophys. Res.*, *107*, doi:10.1029/2002JD002153, in press, 2002.

Patterson, E. M., D. A. Gillette, and B. H. Stockton, Complex index of refraction between 300 and 700 nm for Saharan aerosols, *J. Geophys. Res.*, *82*, 3153–3160, 1977.

Phadnis, M. J., and G. R. Carmichael, Numerical investigation of the influence of mineral dust on the tropospheric chemistry of East Asia, *J. Atmos. Chem.*, *36*, 285–323, 2000.

Pickering, K. E., et al., Convective transport of biomass burning emissions over Brazil during Trace A, *J. Geophys. Res.*, *101*, 23,993–24,012, 1996.

Pickering, K. E., Y. S. Wang, W. K. Tao, C. Price, and J. F. Muller, Vertical distributions of lightning NO_x for use in regional and global chemical transport models, *J. Geophys. Res.*, *103*, 31,203–31,216, 1998.

Piotrowicz, S. R., H. F. Bezdek, G. R. Harvey, M. Springer-Young, and K. J. Hanson, On the ozone minimum over the equatorial Pacific Ocean, *J. Geophys. Res.*, *96*, 18,679–18,687, 1991.

Pochanart, P., J. Kreasuwun, P. Sukasem, W. Geeratithadaniyom, M. S. Tabucanon, J. Hirokawa, Y. Kajii, and H. Akimoto, Tropical tropospheric ozone observed in Thailand, *Atmos. Environ.*, *35*, 2657–2668, 2000.

Price, C., and D. Rind, A simple lightning parameterization for calculating global lightning distributions, *J. Geophys. Res.*, 97, 9919–9933, 1992.

Price, C., J. Penner, and M. Prather, NO_X from lightning, 1, Global distribution based on lightning physics, *J. Geophys. Res.*, 102, 5929–5941, 1997.

Prinn, R. G., et al., Evidence for substantial variations of atmospheric hydroxyl radicals in the past two decades, *Science*, 292, 1882–1888, 2001.

Prospero, J. M., P. Ginoux, O. Torres, and S. E. Nicholson, Environmental characterization of global sources of atmospheric soil dust identified with the Nimbus 7 Total Ozone Mapping Spectrometer (TOMS) absorbing aerosol product, *Rev. Geophys.*, 40(3), 1002, doi:10.1029/2000RG000095, 2002.

Raper, J. L., M. M. Kleb, D. J. Jacob, D. D. Davis, R. E. Newell, H. E. Fuelberg, R. J. Bendura, J. M. Hoell, and R. J. McNeal, Pacific Exploratory Mission in the tropical Pacific: PEM-Tropics B, March–April 1999, *J. Geophys. Res.*, 106(D23), 32,401–32,425, 2001.

Ravishankara, A. R., Heterogeneous and multiphase chemistry in the troposphere, *Science*, 276, 1058–1065, 1997.

Schubert, S. D., R. B. Rood, and J. Pfaendtner, An assimilated data set for Earth Science applications, *Bull. Am. Meteorol. Soc.*, 74, 2331–2342, 1993.

Seidel, D. J., R. J. Ross, J. K. Angell, and G. C. Reid, Climatological characteristics of the tropical tropopause as revealed by radiosondes, *J. Geophys. Res.*, 106, 7857–7878, 2001.

Singh, H., et al., Distribution and fate of select oxygenated organic species in the troposphere and lower stratosphere over the Atlantic, *J. Geophys. Res.*, 105, 3795–3805, 2000.

Singh, H. B., Y. Chen, A. C. Staudt, D. J. Jacob, D. R. Blake, B. G. Heikes, and J. Snow, Evidence from the South Pacific troposphere for large global abundances and sources of oxygenated organic compounds, *Nature*, 410, 1078–1081, 2001.

Spivakovsky, C. M., et al., Three-dimensional climatological distribution of tropospheric OH: Update and evaluation, *J. Geophys. Res.*, 105, 8931–8980, 2000.

Spurr, R. J. D., T. P. Kurosu, and K. V. Chance, A linearized discrete ordinate radiative transfer model for atmospheric remote sensing retrieval, *J. Quant. Spectrosc. Radiat. Transfer*, 68, 689–735, 2001.

Staudt, A. C., D. J. Jacob, J. A. Logan, D. Bachiochi, T. N. Krishnamurti, and N. Poisson, Global chemical model analysis of biomass burning and lightning influences over the South Pacific in austral spring, *J. Geophys. Res.*, 107(D14), 4200, doi:10.1029/2000JD000296, 2002a.

Staudt, A. C., D. J. Jacob, J. A. Logan, D. Bachiochi, T. N. Krishnamurti, and G. W. Sachse, Continental sources, transoceanic transport, and interhemispheric exchange of carbon monoxide over the Pacific, *J. Geophys. Res.*, 106(D23), 32,571–32,590, 2001.

Staudt, A. C., D. J. Jacob, F. Ravetta, J. A. Logan, D. Bachiochi, T. N. Krishnamurti, S. Sandholm, B. Ridley, H. Singh, and B. Talbot, Sources and chemistry of nitrogen oxides over the tropical Pacific, *J. Geophys. Res.*, 107, doi:10.1029/2002JD002139, in press, 2002b.

Thompson, A. M., and R. D. Hudson, Tropical tropospheric ozone (TTO) maps from Nimbus 7 and Earth-Probe TOMS by the modified-residual method: Evaluation with sondes, ENSO signals, and trends from Atlantic regional time series, *J. Geophys. Res.*, 104, 26,961–26,975, 1999.

Thompson, A. M., and J. C. Witte, A new data set for the Earth Science Community, *Earth Obs.*, 11, 27–30, 1999.

Thompson, A. M., K. E. Pickering, D. P. Menamara, M. R. Schoeberl, R. D. Hudson, J. H. Kim, E. V. Browell, V. W. J. H. Kirchoff, and D. Nganga, Where did tropospheric ozone over southern Africa and the tropical Atlantic come from in October 1992?: Insights from TOMS, GTE TRACE A, and SAFARI 1992, *J. Geophys. Res.*, 101, 24,251–24,278, 1996.

Thompson, A. M., B. G. Doddridge, J. C. Witte, R. D. Hudson, W. T. Luke, J. E. Johnson, B. J. Johnson, S. J. Oltmans, and R. Weller, A tropical Atlantic paradox: Shipboard and satellite views of a tropospheric ozone maximum and wave-one in January–February 1999, *Geophys. Res. Lett.*, 27, 3317–3320, 2000.

Thompson, A. M., J. C. Witte, R. D. Hudson, H. Guo, J. R. Herman, and M. Fujiwara, Tropical tropospheric ozone and biomass burning: How related are they?, *Science*, 291, 2128–2132, 2001.

Thompson, A. M., et al., The 1998–2000 SHADOZ (Southern Hemisphere Additional Ozonesondes) tropical ozone climatology: Comparison with TOMS and ground-based measurements, *J. Geophys. Res.*, 107, 10.1029/2001JD000967, in press, 2002.

Torres, O., and P. K. Bhartia, Impact of tropospheric aerosol absorption on ozone retrieval from backscattered ultraviolet measurements, *J. Geophys. Res.*, 104, 21,569–21,577, 1999.

Torres, O., P. K. Bhartia, J. R. Herman, Z. Ahmad, and J. Gleason, Derivation of aerosol properties from satellite measurements of backscattered ultraviolet radiation: Theoretical basis, *J. Geophys. Res.*, 103, 17,099–17,110, 1998.

Wang, H., A. W. Desilva, G. C. Goldenbaum, and R. R. Dickerson, Nitric oxide production by simulated lightning: Dependence on current, energy, and pressure, *J. Geophys. Res.*, 103, 19,149–19,159, 1998.

Wang, Y., D. J. Jacob, and J. A. Logan, Global simulation of tropospheric O_3-NO_X-hydrocarbon chemistry, 1, Model formulation, *J. Geophys. Res.*, 103, 10,713–10,726, 1998a.

Wang, Y., D. J. Jacob, and J. A. Logan, Global simulation of tropospheric O_3-NO_X-hydrocarbon chemistry, 2, Model evaluation and global ozone budget, *J. Geophys. Res.*, 103, 10,713–10,726, 1998b.

Waugh, D. W., and L. M. Polvani, Climatology of intrusions into the tropical upper troposphere, *Geophys. Res. Lett.*, 27, 3857–3860, 2000.

Webster, P. J., and J. R. Holton, Cross-equatorial response to middle-latitude forcing in a zonally varying basic state, *J. Atmos. Sci.*, 39, 722–733, 1982.

Wellemeyer, C. G., S. L. Taylor, C. J. Seftor, R. D. McPeters, and P. K. Bhartia, A correction for Total Ozone Mapping Spectrometer profile shape errors at high latitude, *J. Geophys. Res.*, 102, 9029–9038, 1997.

Weller, R., R. Lilischkis, O. Schrems, R. Neuber, and S. Wessel, Vertical ozone distribution in the marine atmosphere over the central Atlantic Ocean (56°S–50°N), *J. Geophys. Res.*, 101, 1387–1399, 1996.

Wild, O., X. Zhu, and M. J. Prather, Fast-J: Accurate simulation of in- and below-cloud photolysis in tropospheric chemistry models, *J. Atmos. Chem.*, 37, 245–282, 2000.

Yienger, J. J., and H. Levy, Empirical model of global soil-biogenic NO_X emissions, *J. Geophys. Res.*, 100, 11,447–11,464, 1995.

Zhang, Y., and G. R. Carmichael, The role of mineral aerosol in tropospheric chemistry in East Asia—A model study, *J. Appl. Meteorol.*, 38, 353–366, 1999.

Zhang, Y., Y. Sunwoo, V. Kotamarthi, and G. R. Carmichael, Photochemical oxidant processes in the presence of dust: An evaluation of the impact of dust on particulate nitrate and ozone formation, *J. Appl. Meteorol.*, 33, 813–824, 1994.

Ziemke, J. R., and S. Chandra, Seasonal and interannual variabilities in tropical tropospheric ozone, *J. Geophys. Res.*, 104, 21,425–21,442, 1999.

Ziemke, J. R., S. Chandra, A. M. Thompson, and D. P. McNamara, Zonal asymmetries in Southern Hemisphere column ozone: Implications of biomass burning, *J. Geophys. Res.*, 101, 14,421–14,427, 1996.

Ziemke, J. R., S. Chandra, and P. K. Bhartia, Two new methods for deriving tropospheric column ozone from TOMS measurements: Assimilated UARS MLS/HALOE and convective-cloud differential techniques, *J. Geophys. Res.*, 103, 22,115–22,127, 1998.

Ziemke, J. R., S. Chandra, and P. K. Bhartia, Cloud slicing: A new technique to derive upper tropospheric ozone from satellite measurements, *J. Geophys. Res.*, 106, 9853–9867, 2001.

————————

I. Bey and B. N. Duncan, Ecole Polytechnique Federale de Lausanne, CH-1015 Lausanne, Switzerland. (isabelle.bey@epfl.ch; Bryan.Duncan@epfl.ch)

A. M. Fiore, D. J. Jacob, Q. Li, H. Liu, J. A. Logan, R. V. Martin, and R. M. Yantosca, Division of Engineering and Applied Sciences, and Department of Earth and Planetary Sciences, Harvard University, 29 Oxford Street, Cambridge, MA 02138, USA. (amf@io.harvard.edu; djj@io.harvard.edu; qli@io.harvard.edu; hyl@io.harvard.edu; jal@io.harvard.edu; bmy@io.harvard.edu; rvmartin@fas.harvard.edu)

P. Ginoux, Code 916, NASA Goddard Space Flight Center, Greenbelt, MD 20771, USA. (ginoux@rondo.gsfc.nasa.gov)

A. C. Staudt, National Academy of Sciences, 2101 Constitution Avenue, NW, Washington, DC 20418, USA. (AStaudt@nas.edu)

V. Thouret, CNRS (UMR 5560), Laboratoire d'Aérologie, OMP, 14 Avenue E. Belin, F-31400 Toulouse, France. (thov@aero.obs-mip.fr)
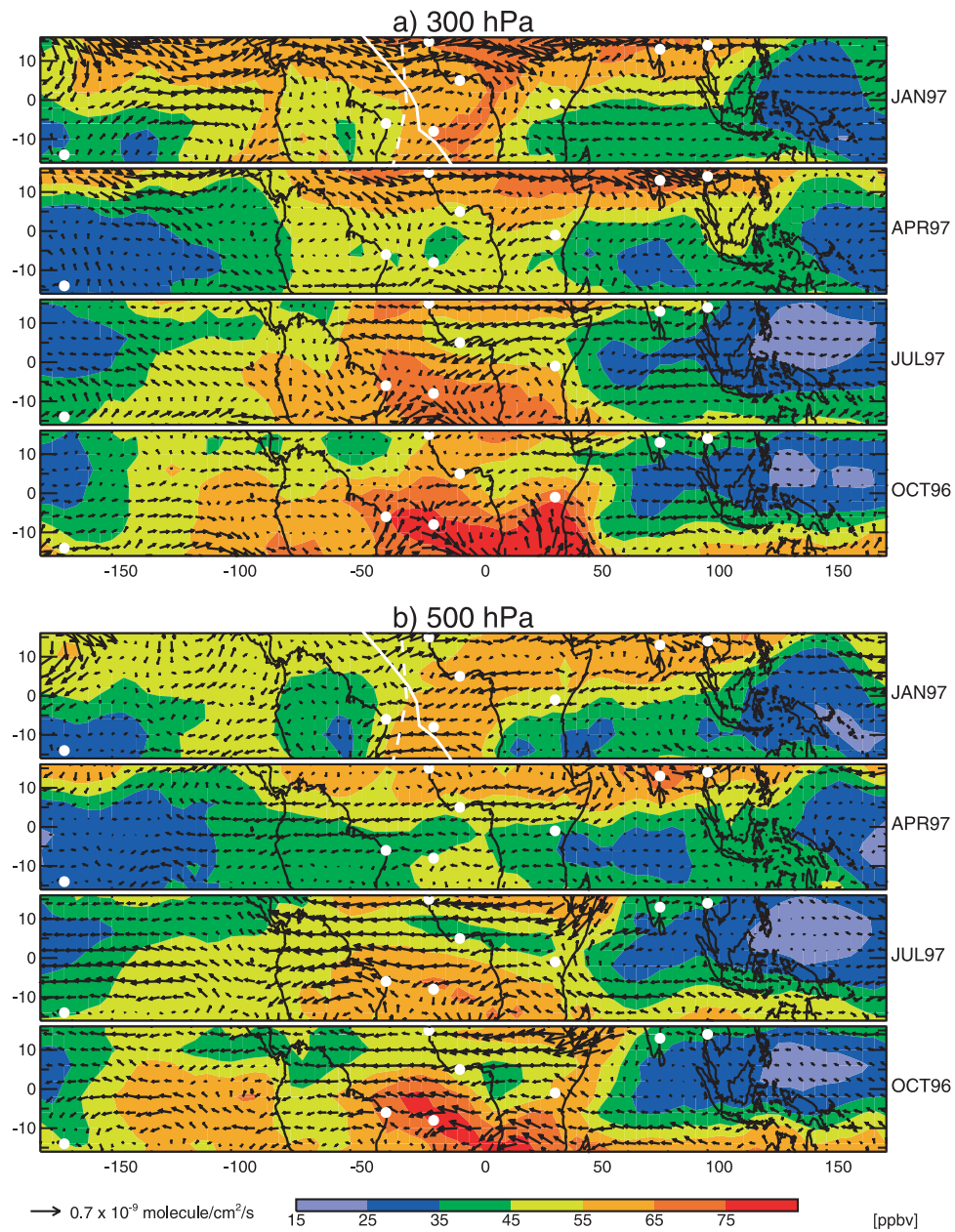
Figure 2. Ozone concentrations and transport fluxes calculated with the GEOS-CHEM model at (a) 300 hPa, (b) 500 hPa, and (c) 800 hPa. White circles show the locations of ozone observations from ozonesondes in the Southern Hemisphere and commercial aircraft in the Northern Hemisphere used to evaluate the model. White lines show ship tracks (Polarstern [*Weller et al.*, 1996] is dashed and Aerosols99 [*Thompson et al.*, 2000] is solid) along which ozonesondes were launched that are used here to evaluate the model.
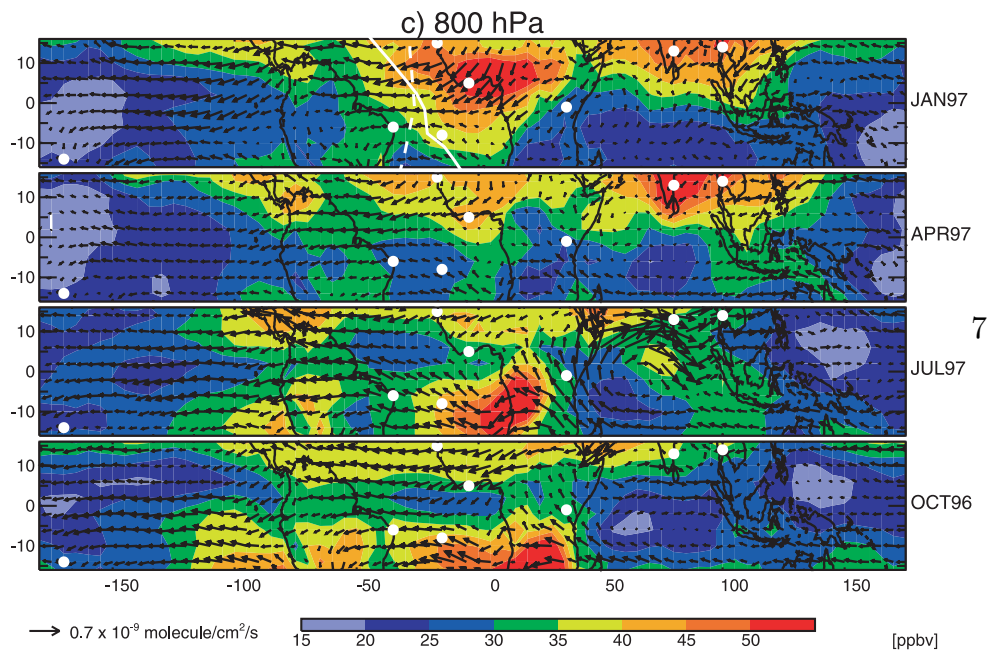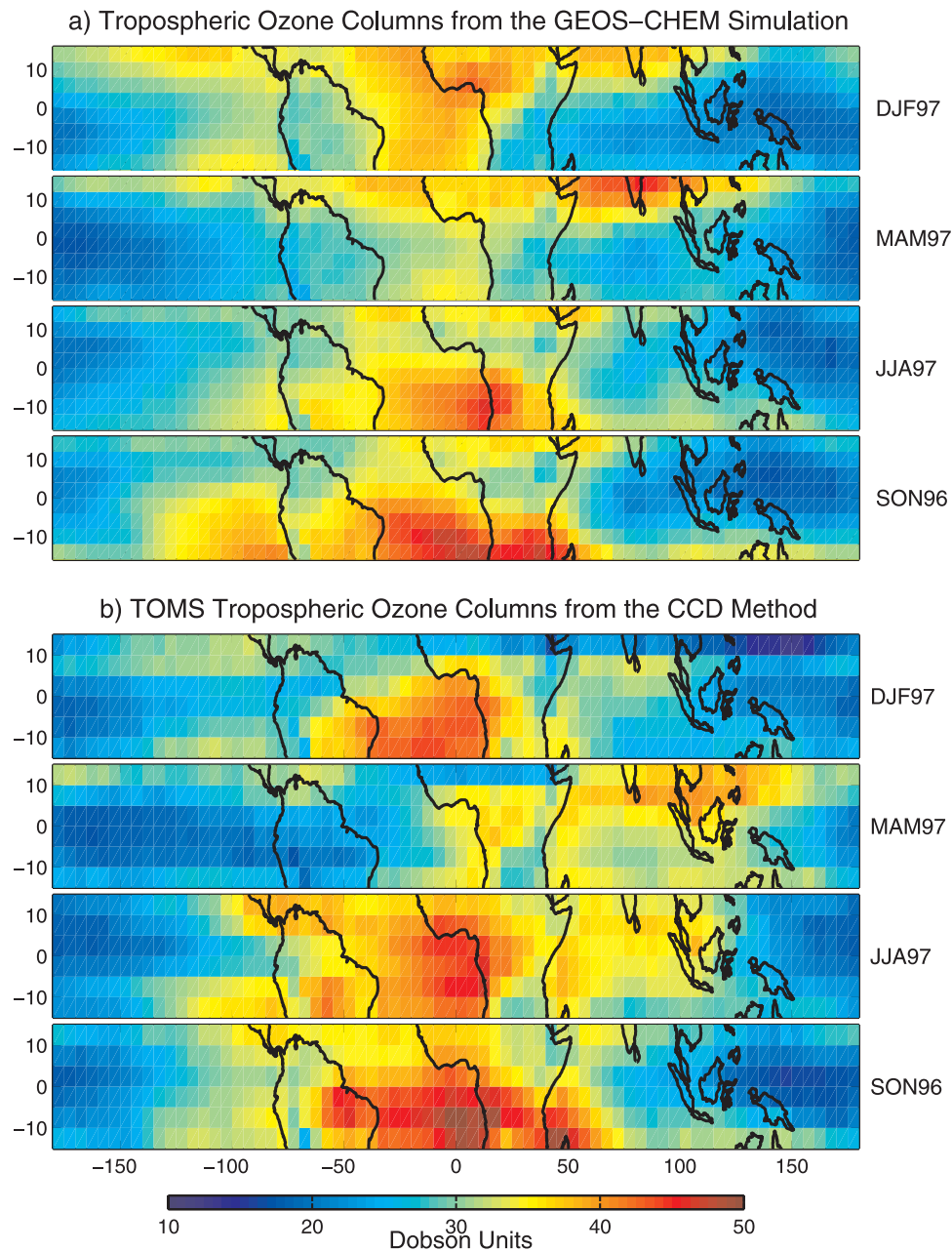
Figure 2. (continued)

Figure 6. Seasonally averaged tropical tropospheric ozone columns (TTOCs) from TOMS for (a) the standard GEOS-CHEM simulation for September 1996–August 1997, (b) the convective cloud differential (CCD) method for September 1996–August 1997 [*Ziemke et al.*, 1998] including the efficiency correction described by *Ziemke et al.* [2001], and (c) The modified residual (MR) method for 1979–1992 [*Thompson and Hudson*, 1999].
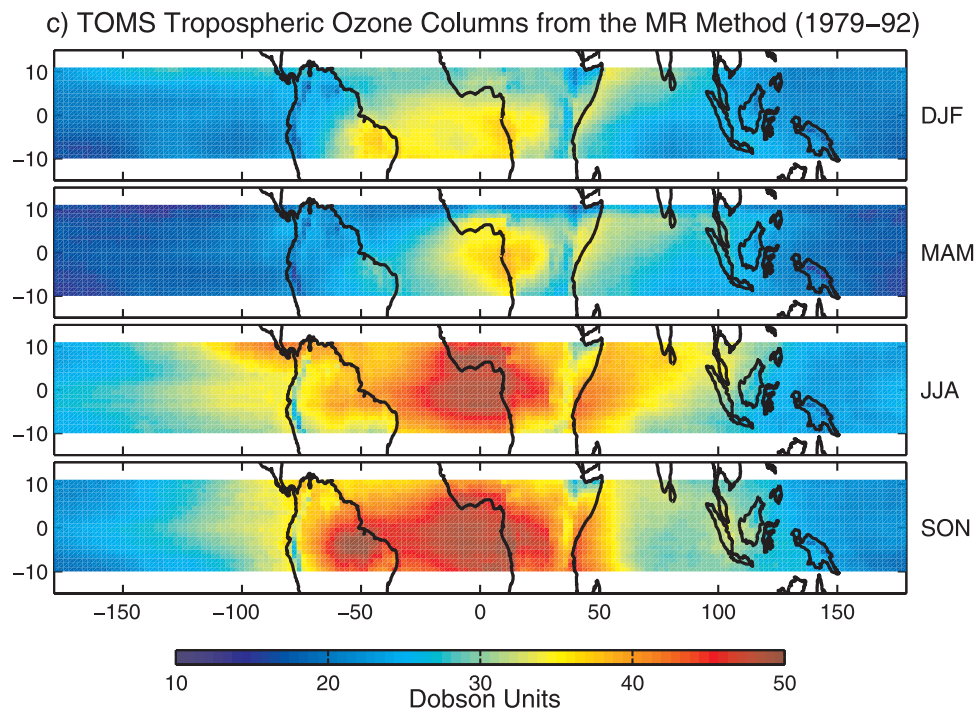
c) TOMS Tropospheric Ozone Columns from the MR Method (1979–92)

Figure 6. (continued)

Figure 12. Seasonally averaged efficiency correction $\Delta\Omega$ (DU) to the TOMS tropospheric ozone column retrievals to account for the insensitivity of the instrument to ozone in the lower troposphere (section 6).

Figure 13. Seasonally averaged tropical tropospheric ozone columns (TTOCs) from TOMS for September 1996–August 1997 [*Ziemke et al.*, 1998] in which the efficiency correction described by *Ziemke et al.* [2001] has been replaced by the efficiency correction presented in Figure 12.
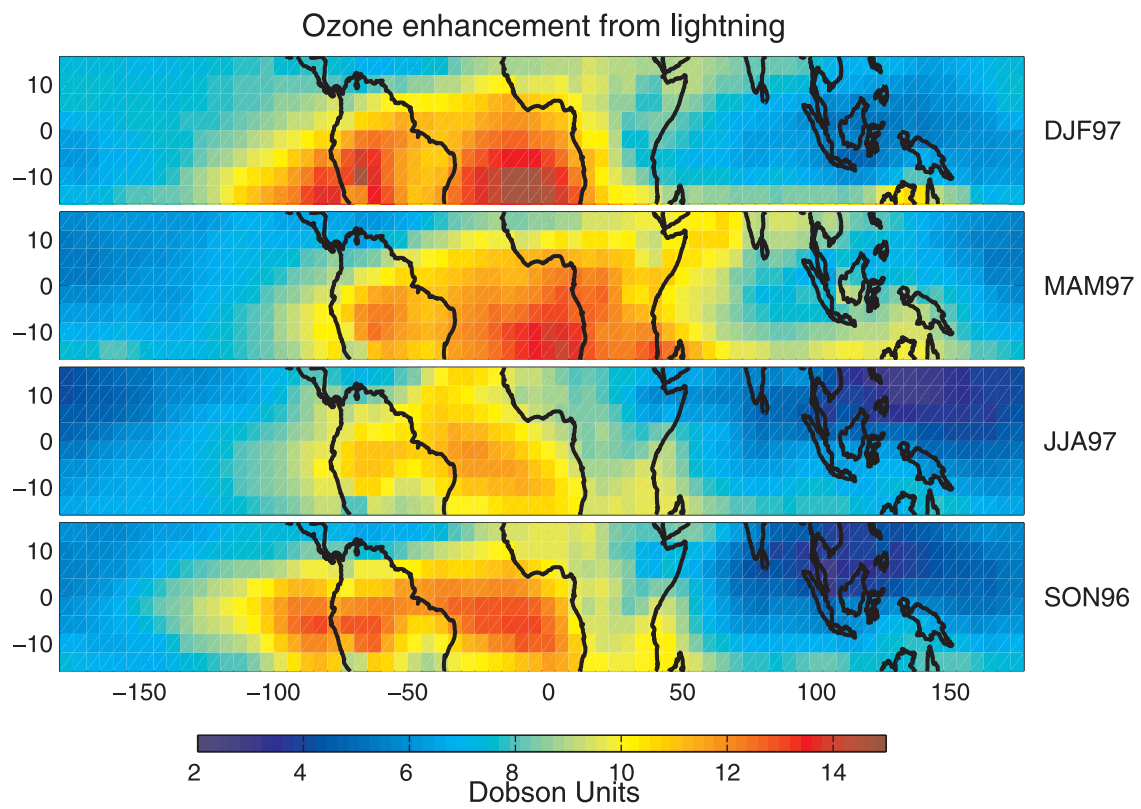
Figure 14. Ozone column enhancement in the GEOS-CHEM model from lightning emissions, as determined by difference from a simulation without lightning emissions.